Comparative Data on the Differentiation and Growth of Bone Ornamentation in Gnathostomes (Chordata: Vertebrata)

Vivian de Buffrénil,[1] François Clarac,[2] Aurore Canoville,[3]* and Michel Laurin[1]

[1]*CR2P (UMR 7207), CNRS/MNHN/UPMC, Département Histoire de la Terre, Muséum National d'histoire Naturelle, Bâtiment de Géologie CC 48, 57 Rue Cuvier F-75231, Paris, Cedex 05, France*
[2]*UPMC Université Paris 06, UMR 7193, Institut des Sciences de la Terre Paris (ISTeP), Sorbonne Universités, 4 Place Jussieu, BC 19, F-75005, Paris, France*
[3]*Steinmann Institute for Geology, Mineralogy and Paleontology, Bonn University, Nußallee 8, Bonn 53115, Germany*

ABSTRACT Bone ornamentation, in the form of rounded pits framed by a network of ridges, is a frequent feature among a great diversity of gnathostome taxa. However, the basic osteogenic processes controlling the differentiation and development of these reliefs remain controversial. The present study is a broad comparative survey of this question with the classical methods used in hard tissue histology and paleohistology. Distinct processes, unevenly distributed among taxa, are involved in the creation and growth of pits and ridges. The simplest one is mere differential growth between pit bottom (slow growth) and ridge top (faster growth). The involvement of several complex remodeling processes, with the local succession of resorption and reconstruction cycles, is frequent and occurs in all major gnathostome clades. Some broad, inclusive clades (e.g., Temnospondyli) display consistency in the mechanisms controlling ornamentation, whereas other clades (e.g., Actinopterygii) are characterized by the diversity of the mechanisms involved. If osteogenic mechanisms are taken into account, bone ornamentation should be considered as a character extremely prone to homoplasy. Maximum likelihood (ML) optimizations reveal that the plesiomorphic mechanism creating ornamentation is differential apposition rate over pits (slow growth) and ridges (faster growth). In some taxas e.g., temnospondyls vs lissamphibians or pseudosuchians, bone ornamentation is likely to be a homoplastic feature due to a convergence process driven by similar selective pressures. ML models of character evolution suggest that the presence of resorption in the development of ornamentation may be selectively advantageous, although support for this conclusion is only moderate. J. Morphol. 000:000–000, 2016. © 2016 Wiley Periodicals, Inc.

KEY WORDS: dermal bone; pits; ridges; histology; bone accretion; bone remodeling

INTRODUCTION

The occurrence of ornamentation (also called sculpture) on the outer surface of the skull roof, mandible, osteoderms and dermal elements of the pectoral girdle, is a common feature in vertebrates (e.g., Vickaryous and Sire, 2009; Witzmann, 2009). It can display diverse aspects, the most common of which, observed in a considerable series of forms, from the Devonian arthrodire placoderms (Miles, 1967; Downs and Donoghue, 2009) to extant archosaurs (Buffrénil et al., 2015), is a pattern of densely-packed pits separated by a network of ridges. These reliefs then form a repetitive motif showing either a honeycomb-like pattern, e.g., the postorbital part of skull roof in crocodiles (Clarac et al., 2015) and the carapace of some turtles, or a partly radiating structure formed by both pits and sub-parallel or slightly divergent grooves framed by ridges, like on the dermal bones of actinopterygians (Lehmann, 1966) and temnospondyls (Bystrow, 1935; Schoch and Milner, 2000, 2014; Witzmann et al., 2010). Considering its striking morphological consistency through time and taxa, this particular type of ornamentation could be viewed as the typical example of a plesiomorphic trait, highly conservative in its morphology. However, the osteogenic mechanisms from which it results seem to be different at least in two groups: the temnospondyls and the pseudosuchians. In the former, ornamentation is supposed to be due to preferential bone accretion on top of the crests (Witzmann, 2009; Witzmann and Soler-Gijón, 2010), a situation shared by the placoderms according to the illustrations found in Downs and Donoghue (2009) and Giles et al. (2013). Conversely, in pseudosuchians, it is mainly created by the excavation of the pits through local bone resorption (Buffrénil et al., 2015; Cerda et al., 2015a). This discrepancy suggests an obvious hypothesis: beyond a superficial phenotypic similarity, ornamentation may not be homologous in all taxa because it involves distinct processes, and might

*Correspondence to: Aurore Canoville; Steinmann Institute for Geology, Mineralogy and Paleontology, Bonn University, Nußallee 8, Bonn 53115, Germany. E-mail: canoville.aurore08@gmail.com

Received 10 December 2015; Revised 10 February 2016; Accepted 12 February 2016.

Published online 00 Month 2016 in Wiley Online Library (wileyonlinelibrary.com).
DOI 10.1002/jmor.20525

have appeared several times in the gnathostomes, through independent, but convergent, evolutionary processes, and under similar selective pressures. This possibility raises the question of the function of bone ornamentation.

In terms of ontogenetic development and growth, the remodeling process involved in the Sphenosuchia as interpreted by Buffrénil (1982) and Buffrénil et al. (2015) is flexible, and prone to quickly adjust pit and ridge dimensions and positions to the overall size of the bones or to any other morphological requirement. Geometrically, this process is submitted to few constraints because of its capacity to erase existing reliefs (either by resorption of crests or by complete filling of depressions) and replace them by new ones. Preferential apposition on ridges looks a priori more constrained in its potentialities because the transformation of bone ornamentation during growth must necessarily be based on, and thus respect, the topography and geometry of pre-existing reliefs. Up to now, very few studies considered this puzzling question specifically, and mentions of it remain anecdotal (e.g., Witzmann and Soler-Gijón, 2010).

This study is intended to present a broad comparative review (based on both original and previously published data) about the osteogenic mechanisms involved in the creation and growth of the reliefs that constitute the pit-and-ridge type of bone ornamentation in gnathostomes. In reference to the results obtained on this topic (and to similar data available in literature and substantiated by clear photographs), the aim is to assess which mechanism produced bone ornamentation in early gnathostomes, especially in actinopterygians, dipnomorphs, and stegocephalians (defined in Laurin [1998], i.e. the largest clade that includes temnospondyls but not panderichthyids; this includes all limbed vertebrates, and possibly a few vertebrates that may have retained paired fins), and how that mechanism changed over time. We also try to determine if one mechanism appears to have a selective advantage over the other. To a lesser extent, our findings have implications about the homology (or lack thereof) of the ornamentation found in various taxa.

MATERIAL AND METHODS

Biological Sample

The biological sample (Table 1) consists of 39 bone samples representing 33 species (12 are nonidentified), distributed in 32 identified genera, 27 families and 12 orders of gnathostomes, according to most recent works that used rank-based nomenclature (we are aware of the subjective nature of these ranks: e.g., Laurin, 2008). Due to sample accessibility, some taxa displaying the pit and ridge ornamentation are not represented in the sample (e.g., early gnathostomes such as the placoderms are lacking). We nevertheless consider that the phylogenetic structure of this sample is an acceptable approximation of the taxonomic diversity of the pit and ridge ornamentation in osteichthyans. Figure 1 shows the ornamental patterns displayed by most of the taxa included in the sample. Collected bones include elements from the skull roof and shoulder girdle, and thus represent typical membrane bones, as well as osteoderms. Both are considered equivalent for the study of the osteogenic processes controlling ornamentation. Bone histology in some of the taxa used in this study has already been described by other authors, especially Florian Witzmann (2009; see also Witzmann and Soler-Gijòn, 2010) for the temnospondyls and Torsten Scheyer (e.g., Scheyer et al., 2012) for the turtles. We nevertheless present additional observations on these taxa since our attention was focussed on very specific details presented according to a relatively standardized framework.

Sample Processing and Histological Observations

For preparing the samples (extant or fossil) into thin sections, the classical techniques used in comparative bone histology (e.g., Lamm, 2013) were employed. Bones from extant taxa were dehydrated in progressive alcohol baths (70 to 100 degrees) and defatted in acetone, while the fossils where simply cleared of sediments when necessary. After photography, all bone samples were embedded in a polyester resin and cut into slices 1 to 3 mm thick. The latter were polished on one side and glued on glass slides to be finally ground into sections 100 μm (± 20 μm) thick. Several sections with varying orientations (e.g., transversal, sagittal) were performed for each bone according to its morphology, in order to assess structural details that depend on sectional orientation such as the morphology of osteocyte lacunae or the refringence properties of the bone matrix in polarized light. Observations were made with a Zeiss Axioskop 40 microscope, equipped for polarization. Measurements of bone compactness (i.e., actual area occupied by bone tissue expressed as a percent of total sectional area) were performed on digitized images of the sections with the software ImageJ (National Institute of the Health, USA). All the sections are presently housed and numbered in the HISTOS collection of the Muséum National d'Histoire Naturelle, Paris, France.

Basic Clues for Interpreting Relative Bone Growth Rates

The interpretations developed in this study are based on an assessment, at least in relative terms, of the rate of local bone accretion from the fine structure of the osseous tissue. For this purpose we refer, on the one hand, to the typology and nomenclature of bone tissues proposed by Francillon-Vieillot et al. (1990) and, on the other hand, to the results of experimental studies on the relationships between growth rate and bone structure (e.g., Amprino, 1947; Castanet et al., 1996, 2000; Margerie et al., 2002, 2004; Cubo et al., 2012; Kolb et al., 2015), which are broadly acknowledged, as shown by the fact that they have been used to infer growth rates in extinct taxa (e.g., Padian, 2013; Amson et al., 2015). In brief, apposition rate positively influences the three following features of bone tissue, and is grossly correlated with them:

1. Degree of birefringence of the intercellular collagenous matrix. Low birefringence, or *a fortiori* complete monorefringence, reveals a poorly structured collagen meshwork, that is, the "woven-fibered" matrix. This is a typical trait of fast-growing periosteal cortices (growth speed: 15–170 μm/day, according to Castanet et al., 1996, 2000; Margerie et al., 2002, 2004). When growth rate decreases, bone matrix progressively turns into the "parallel-fibered" organization that provokes a "mass birefringence" in polarized light, and corresponds to growth speeds of 2–20 μm/day (Margerie et al., 2002). With further decrease in growth speed, bone matrix becomes "lamellar", with a subdivision into strata of some 3–5 μm in thickness that appear alternatively dark and illuminated in polarized light. Each stratum is composed of parallel-fibered tissue, but the directions of the fibres in adjacent strata are approximately orthogonal. Corresponding growth rates are 0.2–2.5 μm/day (Margerie et al., 2002).

TABLE 1. Biological and paleontological samples used in this study

Higher taxon	Family	Genus	Species	Bone	Geol. age	Coll. number
ACTINOPTERYGII						
Acipenseriformes	Acipenseridae	*Acipenser*	*sturio*	Opercular	Extant	UPMC-JYS. A.s. 2
Neopterygii						
Siluriformes	Pimelodidae	*Phractocephalus*	*hemioliopterus*	Opercular	Extant	MAE-USP. PN 13-831-4
Siluriformes	Ariidae	*Sciades*	*proops*	Opercular	Extant	MNHN-AC/ET. 0018
Osteoglossiformes	Osteoglossidae	*Arapaima*	*gigas*	Opercular	Extant	MNHN-AC/ET. 0034
SARCOPTERYGII						
Porolepiformes	Holoptychidae	*Holoptychius*	*quebecensis*	Scute	U. Dev.	MNHN-F. no number
Stegocephali						
Temnospondyli	Eryopidae	*Eryops*	*megacephalus*	Indet. skull bone	E. Perm.	UPMC-AR.I1/b35
Temnospondyli	Trimerorachidae	*Trimerorachis*	*insignis*	Indet. skull bone	E. Perm.	UPMC-AR.I1/b2
Temnospondyli	Peltobatrachidae	*Peltobatrachus*	sp.	Osteoderm	U. Perm.	MNHN-F. no number
Temnospondyli	Archegosauridae	*Platyoposaurus*	sp.	Indet. skull bone	U. Perm.	UPMC-AR.I2/b11
Temnospondyli	Benthosuchidae	*Benthosuchus*	*sushkini*	Indet. skull bones	E. Trias.	UPMC-AR. I2/b12
Temnospondyli	Metoposauridae	*Dutuitosaurus*	*ouazzoui*	Jug., interclav.	U. Trias.	MNHN-F. AZA 395
Temnospondyli	Metoposauridae	Indet.	sp.	Indet. skull bone	U. Trias.	UPMC-AR. I2/b3
Temnospondyli	Capitosauridae?	*Kupferzellia*	sp.	Postpar.	M. Trias.	SMNS 54673
Temnospondyli	Mastodonsauridae	*Mastodonsaurus*	sp.	Par.	M. Trias.	SMNS 81063
Temnospondyli	Mastodonsauridae	*Parotosuchus*	sp.	Indet. skull bone	E. Trias.	MNHN-F. R13.Z16
Temnospondyli	Plagiosauridae	*Plagiosternum*	sp.	Interclav.	M. Trias.	SMNS No number
Temnospondyli	Plagiosauridae	*Plagiosuchus*	sp.	Postpar.	M. Trias.	SMNS 91040
Temnospondyli	Capitosauridae	*Stanocephalosaurus*	sp.	Indet. skull bones	M. Trias.	MNHN-F. Zar. 41, 59, 63
Embolomeri	Archeriidae	*Archeria*	sp.	Osteoderm	E. Perm.	UPMC-R. I1/b30
Chroniosuchia	Bystrowianidae	*Bystrowiana*	cf. *permiria*	Indet. skull bone	U. Perm.	UPMC-AR. I2/b18
Nectridea	Keraterpetontidae	*Diplocaulus*	sp.	Indet. skull bones	E. Perm.	UPMC-AR. I1/b20-22
Anura	Ceratophryidae	*Ceratophrys*	*cornuta*	Skull roof	Extant	MNHN-F.GR 21
Anura	Natatanura	*Thomastosaurus*.	*gezei*	Max., Fr-Par., Sq.	U. Eoc.	MNHN-F. MALP.1-3
Anura	Alytidae	*Latonia*	*gigantea*	Fr-par., max.	M. Mioc.	MNHN-F. Sa 23489, 23468
Amniota						
Sauropsida	Captorhinidae	*Captorhinus*	*aguti*	Indet. skull bones	E. Perm.	UPMC-AR. I4/b6
Testudines	Trionychidae	*Amyda*	*cartilaginea*	Carapace plate	Extant	MHNL 50.000.1357
Testudines	Trionychidae	*Trionyx*	*triunguis*	Carapace plate	Extant	MNHN-AC.1889.384
Testudines	Trionychidae	*Trionyx*	*triunguis* foss.	Carapace plate	Pleist.	MNHN-F. MN 16
Testudines	Trionychidae	*Aspideretoides*	cf. *riabinini*	Carapace plate	U. Cret.	MNHN-F. no number
Testudines	Trionychidae	*Cyclanorbis*	*senegalensis*	Carapace plate	Extant	MNHN-F. AR 76
Testudines	Emydidae	*Pseudemys*	*rubriventris*	Carapace plate	Extant	MNHN-F. no number
Testudines	Araripemydidae	*Araripemys*	*barretoi*	Carapace plate	E. Cret.	MNHN-F. no number
Squamata	Necrosauridae	*Necrosaurus*	*cayluxensis*	Osteoderms	Eoc.	MNHN-F. QUER.4
Synapsida	Edaphosauridae	*Lupeosaurus*	*kayi*	Indet. skull bone	E. Perm.	UPMC-AR. I7/b8

Meaning of the abbreviations: MAE-USP. PN: Museo de Arqueologia de Universidade de São Paulo – Paraná; MHNL: musée des Confluences, centre de conservation et d'étude des collections, Lyon, France; MNHN-AC, or F: Collections of comparative anatomy (AC) or vertebrate paleontology (F) of the Muséum National d'Histoire Naturelle (Paris, France); SMNS: Staatlisches Museum Naturkunde Stuttgart (Germany); UPMC-AR: Armand de Ricqlès' collections in Université Pierre et Marie Curie (Paris, France); UPMC-JYS: Jean-Yves Sire's collection in Université Pierre et Marie Curie (Paris, France). Abbreviations for geological ages: Dev.: Devonian; E: Early; Eoc.: Eocene; M: Middle; Mioc.: Miocene; Perm.: Permian, Pleist.: Pleistocene; Trias.: Triassic, and U: Upper. Abbreviations for bones sampled: Fr-Par.: fronto-parietal; Interclav.: interclavicle; Jug.: jugal; Max.: maxillary; Par.: parietal; Postpar.: postparietal; Sq.: squamosal; Indet.: undetermined.
Some of our material was labeled as "*Cricotus* sp.," but we follow Holmes (1989) in considering *Cricotus* as a synonym of *Archeria*. Similarly, one of our turtle specimens was registered as *Palaeotrionyx*, a name now considered synonym of *Aspideretoides* cf. *riabinini* (Danilov and Vitek, 2013).

Matrix structure changes gradually from the woven-fibered to the lamellar types when bone depositional rate decreases.

2. Aspect of cell lacunae. Globular or multipolar cell lacunae that may display abundant canaliculi (but this condition is not mandatory) are associated with woven-fibered matrices and thus indicative of fast-growing cortical bone. Conversely, spindle-like or flat cell lacunae (with variable canalicular development) are typically encountered in parallel-fibered or lamellar tissues, and therefore reveal relatively slow growing bone.
3. The density of vascular canals is positively correlated with appositional rate, and can reflect localized acceleration or deceleration of periosteal accretion (Castanet et al., 1996; Margerie et al., 2002, 2004). Moreover, the orientation of the canals (longitudinal, oblique, radial, etc.) is also linked to bone growth rates, but with apparently more complex, and still incompletely elucidated, interactions (cf. Margerie et al., 2002); this is why this last feature (canal orientation) will not be considered in this study. Morphologically, simple vascular canals, when cut transversely, are easily distinguished from cell lacunae, or other possible "holes" contained in bone matrix, by their diameter that is most often larger than 10 μm and their sharp and smooth contour. When cut obliquely or longitudinally, they appear like sharply defined tubes that cannot be confused with anything else.

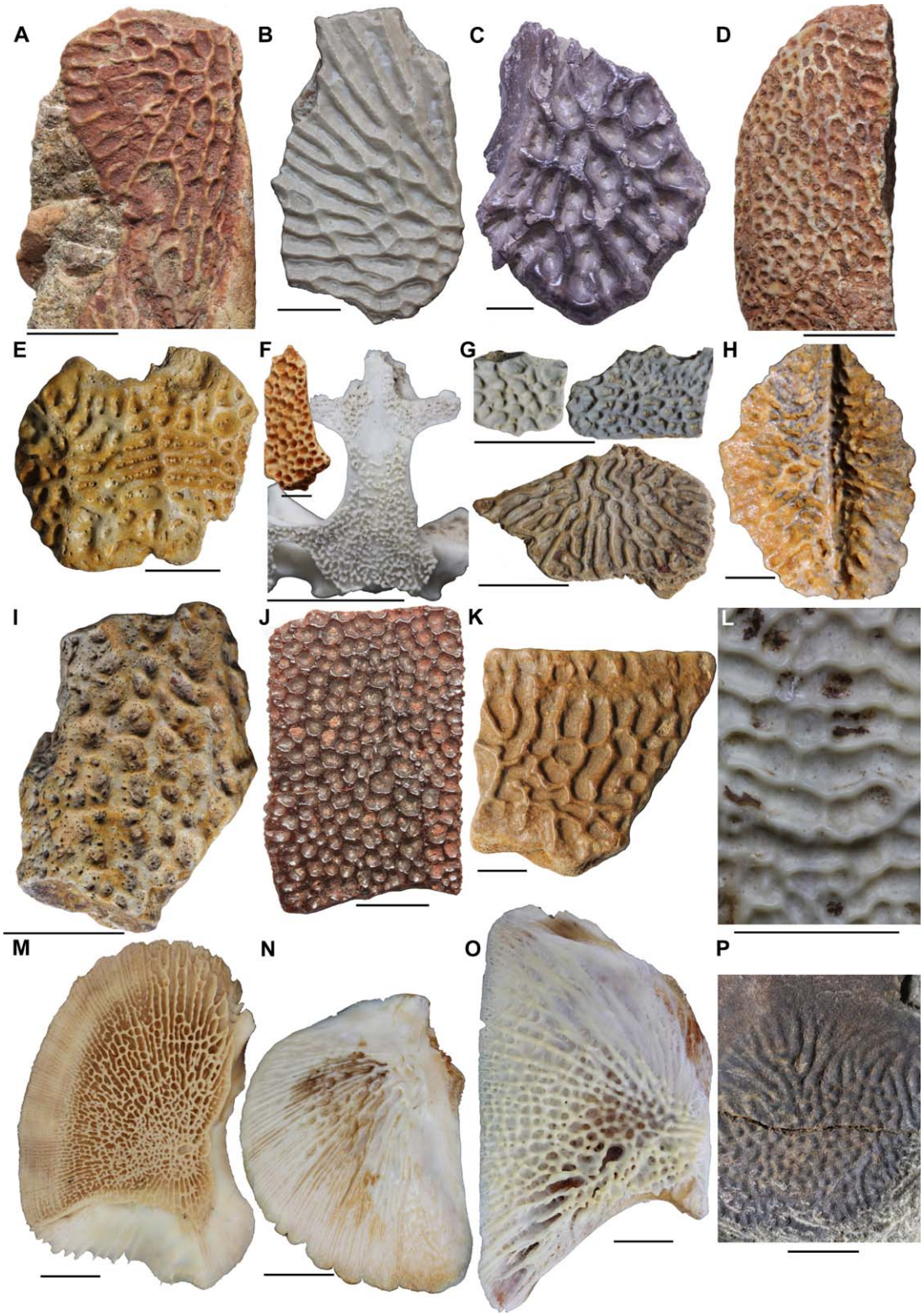

Fig. 1. Morphology of the pit and ridge ornamentation type in the biological sample. **A**: Undetermined skull bone of the Early Triassic *Benthosuchus sushkini* (Temnospondyli). **B**: Undetermined skull bone of the Early Triassic *Stanocephalosaurus* (Temnospondyli). **C**: Fragment of postparietal of the Middle Triassic (Ladinian) *Kupferzellia* (Temnospondyli). **D**: Undetermined skull bone of the Early Permian *Diplocaulus* sp. (Nectridea). **E**: Osteoderm of the Late Permian *Bystrowiana* cf. *permiria* (Chroniosuchia). **F**: Calvarium of the extant *Ceratophrys cornuta* (Anura), with detail of the fronto-parietal of the Eocene *Thaumastosaurus* from the Quercy Phosphorites. **G**: Fragments of undetermined skull bones of the Early Permian amniote *Captorhinus aguti* (upper half) and osteoderm of the Early Permian embolomere *Archeria* (lower half). **H**: Osteoderm of an undetermined Eocene *Necrosaurus* (Squamata) from the Quercy Phosphorites. **I**: Undetermined skull bone of the Early Permian synapsid *Lupeosaurus kayi* (Edaphosauridae, Eupelycosauria). **J**: Carapace fragment of the Early Cretaceous *Araripemys barretoi* (Testudines). **K**: Carapace fragment of the Paleocene *Palaeotrionyx sp*. (Testudines). **L**: Detail of the plate from the carapace of the extant *Amyda cartilaginea* (Testudines). **M**: Opercular of the extant *Acipenser sturio* (Actinopterygii: Acipenseriformes). **N**: Opercular of the extant *Arapaima gigas* (Actinopterygii: Osteoglossiformes). **O**: Opercular of the extant *Sciades proops* (Actinopterygii: Siluriformes). **P**: Scale of the Devonian *Holoptychius* cf. *quebecensis* (Sarcopterygii: Porolepiformes). Scale bars: 1 cm, except for H = 1 mm; M, N = 2 cm.

Reference Phylogeny

A reference phylogeny was compiled from the literature. It attempts to capture the current consensus about topology and divergence times, although some controversies make this exercise difficult. This is especially true of the position of turtles. Therefore, all evolutionary analyses reported below are based on two trees: one in which turtles are located outside Diapsida, as several paleontological studies have suggested (Laurin and Reisz, 1995; Lee, 2001; Lyson et al., 2010), and another in which they are located in Diapsida, as basal archosauromorphs, as suggested by several recent molecular studies (e.g., Hugall et al., 2007; Chiari et al., 2012). Several recent paleontological studies have also placed turtles within diapsids, typically among lepidosauromorphs (e.g., Rieppel and Reisz, 1999; Schoch and Sues, 2015), but an archosauromorph placement is apparently not too unparsimonious from a morphological point of view (Lee, 2013). And to complicate things further, some molecular studies placed turtles among lepidosauromorphs (e.g., Lyson et al., 2012), but we believe that the two selected reference trees summarize well the bulk of the literature on this topic.

Most other taxa were far easier to place, including those within turtles, for which the topologies follow Guillon et al. (2012) for extant taxa, and Sterli et al. (2013) for extinct ones. Stegocephalian phylogeny follows Vallin and Laurin (2004), except for the position of chroniosuchians, which follows Schoch et al. (2010). The phylogeny of temnospondyls follows Schoch (2008, 2013), except for *Peltobatrachus*, which was placed following Eltink and Langer (2014).

The position of lissamphibians (the smallest clade that includes all extant amphibians) is controversial. For most of the 20th century, most authors have considered them to be nested within temnospondyls (e.g., Bolt, 1969; Ruta and Coates, 2007; Sigurdsen and Green, 2011), but several analyses involving one of us (M.L.) have recently supported a position in lepospondyls instead (e.g., Laurin, 1998; Vallin and Laurin, 2004; Marjanović and Laurin, 2013), a result also obtained by Pawley (2006) in one of her analyses. However, this controversy has very little impact on our study because under all recently published phylogenies, their sister-group among the sampled taxa lack remodeling in the process leading to dermal ornamentation. Thus, to avoid complicating needlessly the analyses we placed lissamphibians (represented only by anurans, in our sample) among "lepospondyls" (here represented solely by *Diplocaulus*).

The tree was time-scaled using the Stratigraphic Tools (Josse et al., 2006) of Mesquite (Maddison and Maddison, 2014) using both paleontological (stratigraphic age) and molecular divergence dates, many of which were obtained from Kumar and Hedges (2011).

Evolutionary Analyses

To assess the ancestral condition for gnathostomes, stegocephalians, sauropsids and other clades present in our tree, as well as to reconstruct character history, we performed maximum likelihood (ML) optimizations. This has a few advantages compared with the maximum parsimony (MP) optimizations. First, the ML optimization (Pagel, 1999) uses branch lengths, which are approximately known in the case of paleontological trees because fossils bear temporal information. MP (Swofford and Maddison, 1987) typically neglects branch length information. Second, ML optimization can yield probabilities that each state was present at a given node, rather than a single most parsimonious state, or a set of equally parsimonious states. In both cases, the parsimony solution is suboptimal because even if a single most parsimonious solution exists for a given node, it is not necessarily the actual condition that existed in the last common ancestor (Oakley and Cunningham, 2000; Webster and Purvis, 2002; Bollback, 2006; Germain and Laurin, 2009). Moreover, when a set of equally parsimonious states exists, each state comprised in the set is probably not equally well-supported. Third, ML analysis can reveal asymmetries in transition rates (between states 0 and 1) better than MP analysis because it assesses these through evolutionary models to yield best estimates of both (forward and backward) rates. By contrast, MP often yields ambiguous optimizations on part of the tree, which complicate assessment of transition rates (e.g., Smith et al., 2013).

Support for each ML model was assessed by converting their log-likelihood into AIC weights, using formulae given in Wagenmakers and Farrell (2004) and that involve computing AICc (for small samples) as an intermediate step. This is generally preferable to using the older log-likelihood ratio test because the number of estimated parameters often differs between the compared models (as is the case here), and this complicates interpretation of the log-likelihood ratio test (Wagenmakers and Farrell, 2004). The two usual models (a one-rate and a two-rate model) were assessed in Mesquite 3.04 (Maddison and Maddison, 2014). Below, we report results from each model, as well as a weighted average of values (probabilities of each state at selected nodes) yielded by both models. These are weighted by the AIC weights of each model. This is done for both reference phylogenies (differing in the position of turtles).

For two nodes and characters that appeared particularly relevant (Sauropsida and Actinopterygii), we have calculated model-averaged probabilities of the states. These nodes were selected because their condition is particularly uncertain (the exercise would have been trivial in most other cases because the probability of the most likely state exceeded 99.9%). This was done under two topologies (differing by the position of turtles, inside or outside diapsids).

RESULTS

Stegocephali

Temnospondyli, Lepospondyli (*Diplocaulus*), and Chronosuchia (*Bystrowiana*).

General structural features of ornamented bones. The general micro-anatomic and histological structure of temnospondyl ornamented bones shows substantial variability between taxa, but some general characteristics (and a few atypical situations) can be distinguished, at least in the taxa for which the quality of preservation of the fossils allows detailed observations. These characteristics are shared with the nectridean (lepospondyl) *Diplocaulus* and the chroniosuchian *Bystrowiana*; these taxa are thus included in the following description.

Most bones have a gross diploe architecture, with two compact periosteal cortices framing a cancellous core (Fig. 2A–H). However, the compactness of the core region is extremely variable between specimens, and the resulting global compactness of the sampled bones ranges from 69.6% for the bone of *Trimerorachis* (Fig. 2E) to 87.7% for the interclavicle of *Plagiosternum* (Fig. 2C). When present, the basal cortex is made of variably birefringent parallel-fibered bone. Vascularization is generally sparse in this tissue, but several exceptions exist, mainly the parietal of *Mastodonsaurus* that displays abundant primary osteons organized in parallel strata, the interclavicle of *Plagiosternum*, the postparietal of *Plagiosuchus* and, to a lesser extent, the bone of *Eryops*. The core region, be it of high or low compactness, is always heavily remodeled (Fig. 2I,J), and the local spongiosa is thus secondary (at least for most of its volume). Remodeling is so intense in most specimens that no trace of the primary tissue once present locally persists. In

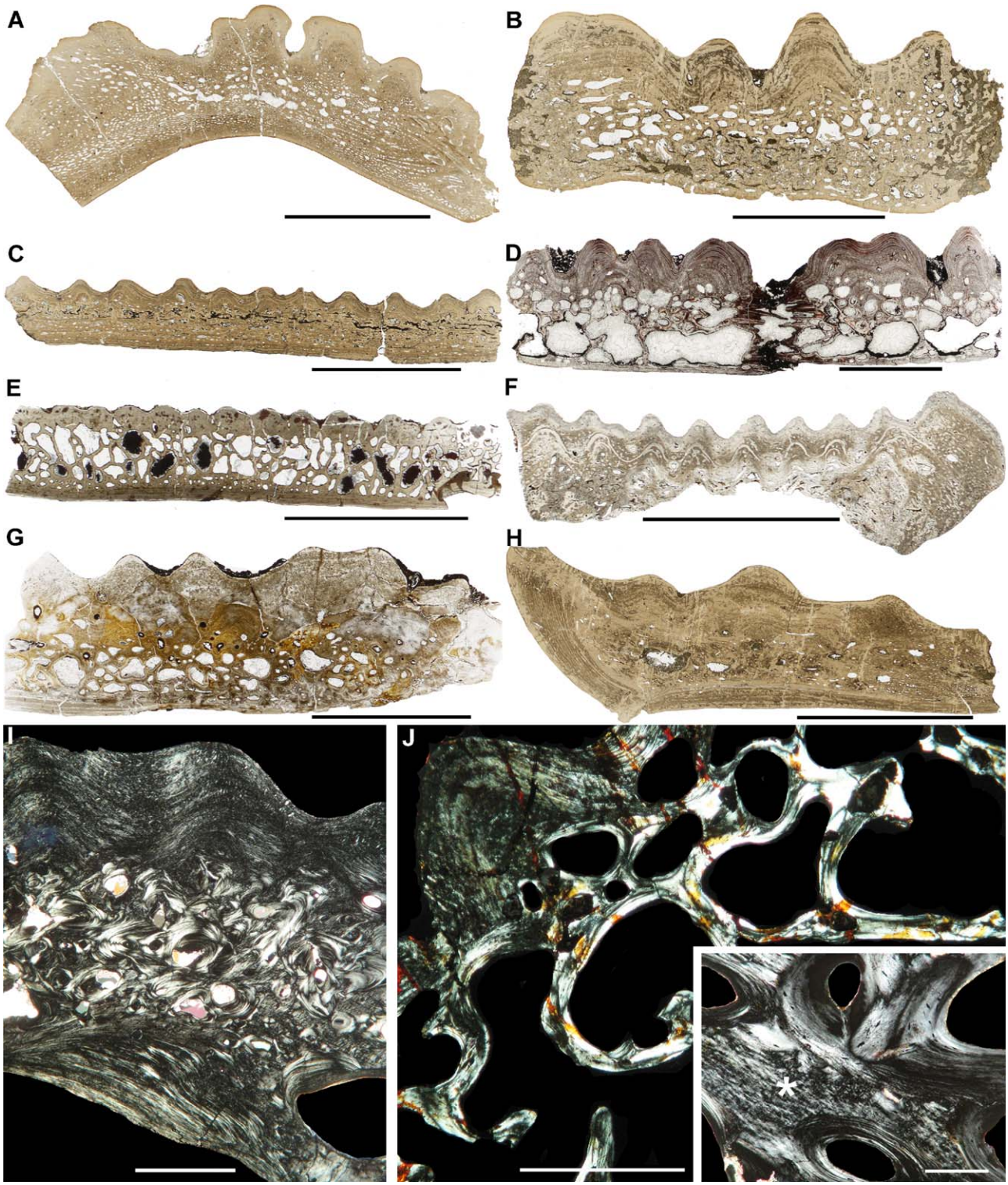

Fig. 2. General structure of ornamented bones in the Temnospondyli (cross sections). **A**: Postparietal of a Middle Triassic *Plagiosuchus* sp. **B**: Postparietal of a Middle Triassic *Kupferzellia* sp. **C**: Interclavicle of a Middle Triassic *Plagiosternum* sp. **D**: Interclavicle of the Late Triassic *Dutuitosaurus ouazzoui*. **E**: Undetermined skull bone of an Early Permian *Trimerorachis* sp. **F**: Skull bone of the Middle Triassic *Stanocephalosaurus*. **G**: Skull bone of an undetermined Late Triassic metoposaur. **H**: Parietal of a Middle Triassic *Mastodonsaurus* sp. **I**: General structure of an undetermined bone of *Platyoposaurus*, viewed in transmitted polarized light. The superficial (ornamented), and basal cortices are made of parallel-fibered tissue; the core of the bone is a tight spongiosa intensely remodeled. **J**: Loose, remodeled central spongiosa in a Late Permian *Peltobatrachus* osteoderm. Insert: Primary woven-fibered-like tissue (asterisk) persisting in the remodeled central spongiosa of a Middle Triassic *Kupferzellia* postparietal. Scale bars: 1 cm, except for I, J (main frame) = 1 mm; J (insert) = 0.2 mm.

the specimens of *Kupferzellia* (Fig. 2J, insert), *Plagiosuchus*, *Parotosaurus*, *Platyoposaurus*, and *Stanocephalosaurus*, the remnants of this tissue, less eroded by remodeling and better preserved by fossilization than in other specimens, display histological features intermediary between parallel-fibered bone (birefringence of bone matrix, though faint and irregular) and woven-fibered bone (multipolar cell lacunae randomly oriented).

The superficial, ornamented cortex also shows structural consistency between taxa but, again, a few peculiar conditions exist. In most specimens, the bottom of the pits is covered by a layer of parallel-fibered bone tissue, comprising spindle-like osteocyte lacunae, oriented parallel to the bone surface, and a birefringent matrix (Fig. 3A,B). Depending on the taxa, this tissue may (in e.g., the *Stanocephalosaurus* bone shown in Fig. 3C or the osteoderm of *Bystrowiana*), or may not (e.g., *Diplocaulus*: Fig. 3B,D) extend into the core of the ridges framing the pits. It is often devoid of vascularization (Fig. 3A,B), but this situation is far from being general, and simple vascular canals or primary osteons (Fig. 3C,E) may occur. Similarly, Sharpey's fibers can occasionally be present in the layers forming the bottom of the pits. Ridges often display a stratified structure characterized by the alternation of well-vascularized (by simple canals or primary osteons) monorefringent or poorly birefringent strata, and avascular birefringent ones similar to *annuli*, as exemplified by *Kupferzellia* (Fig. 3F) or *Mastodonsaurus*. The bone layers located at the base or in the core of the ridges display relatively dense vascularization that decreases toward the cortical periphery (Fig. 3G). Sharpey's fibers are frequent in the apices of the ridges (e.g., Fig. 3B). The main exception to this general pattern is represented by two skull bones (one is from a small specimen, and the other from a much larger one) of *Benthosuchus sushkini* (Fig. 3H) that display ridges made of a poorly birefringent tissue devoid of cyclic growth marks and densely vascularized by a reticular network of simple vascular canals.

All temnospondyl sections share an important common feature: the superficial bone layers located either in the floor of the pits or in the walls of the ridges never contain reversion lines, discordant bone deposits or superficial traces of resorption such as Howship's lacunae. These bone layers are thus entirely made of primary tissues in continuity with, though eventually different in structure from, subjacent bone strata. There is no superficial remodeling (resorption and reconstruction cycles) in temnospondyl ornamented bones, as well as in the bones of *Diplocaulus* and *Bystrowiana* used in this study.

Dynamic processes in superficial cortices Superficial cortices of temnospondyl (and other basal stegocephalians) ornamented bones show evidence of an active modeling process that typically excludes a previous resorption stage. Ornamentation growth can be observed only in relatively peripheral layers because deep cortical strata are generally submitted to extensive resorption and reconstruction, as mentioned above. The pattern and spacing of cyclical growth marks, along with the distribution and density of vascular canals and the refringence characteristics of bone matrix in polarized light, suggest that the overall geometry of bone ornamentation (i.e., pit and ridge shapes and dimensions), is exclusively influenced during growth by local differences in apposition rate and slight shifts in the direction of bone deposits. Six main situations, which may occur simultaneously on a single bone, are frequently observed:

1. Simple, local piling of bone reliefs during growth (Figs. 2B,D,F, 3C, and 4A). This situation may occur in all taxa, and was most clearly observed in a cranial bone of *Stanocephalosaurus* (Fig. 3C), in a *Dutuitosaurus* supratemporal (Fig. 4A), and in the middle region of an osteoderm of *Bystrowiana*. Periosteal bone accretion results in a mere superposition of bone reliefs, with no significant modification in the width or position of pits and ridges from one growth stage to the following one. The apices of the ridges, as well as the center of the pits, do not present any significant drift; therefore, the absolute diameter of individual pits remains constant during growth. Conversely, in relative terms, pit widths tend to decrease as compared to the augmenting size of the bones that bear them. The bottom of the pits may rise in pace with the top of the ridges (e.g., Fig. 3C), or at a slower rate (Fig. 4A). In the first case, pit shape remains unchanged during growth, whereas in the second case, pits tend to become relatively deeper and narrower.
2. Symmetric ridge drift (Fig. 4B). The apices of the ridges that frame an individual pit tend to diverge symmetrically from each other during growth, as a consequence of a lateral off-centering of periosteal deposits on top of the ridges. Opposite to the simple, centered piling described above, this process results in a progressive increase in pit diameter. However, it also tends to constrain the diameters of neighboring pits, and contributes to the *total ridge drift* described below. This growth pattern was observed on the supratemporal of *Dutuitosaurus*, the interclavicle of *Plagiosternum*, the postparietal of *Plagiosuchus*, and the skull bones of *Eryops* (Fig. 4B) and *Stanocephalosaurus*.
3. Total ridge drift (Fig. 4C). The ridges around a given pit migrate in the same direction (i.e., toward the lateral margins of the bone), as a result of similar and parallel off-centering of periosteal bone accretion. Slight differences in the rates of these processes can result in some local widening of the pits during growth (as shown on Fig. 4C), but potentially also in some

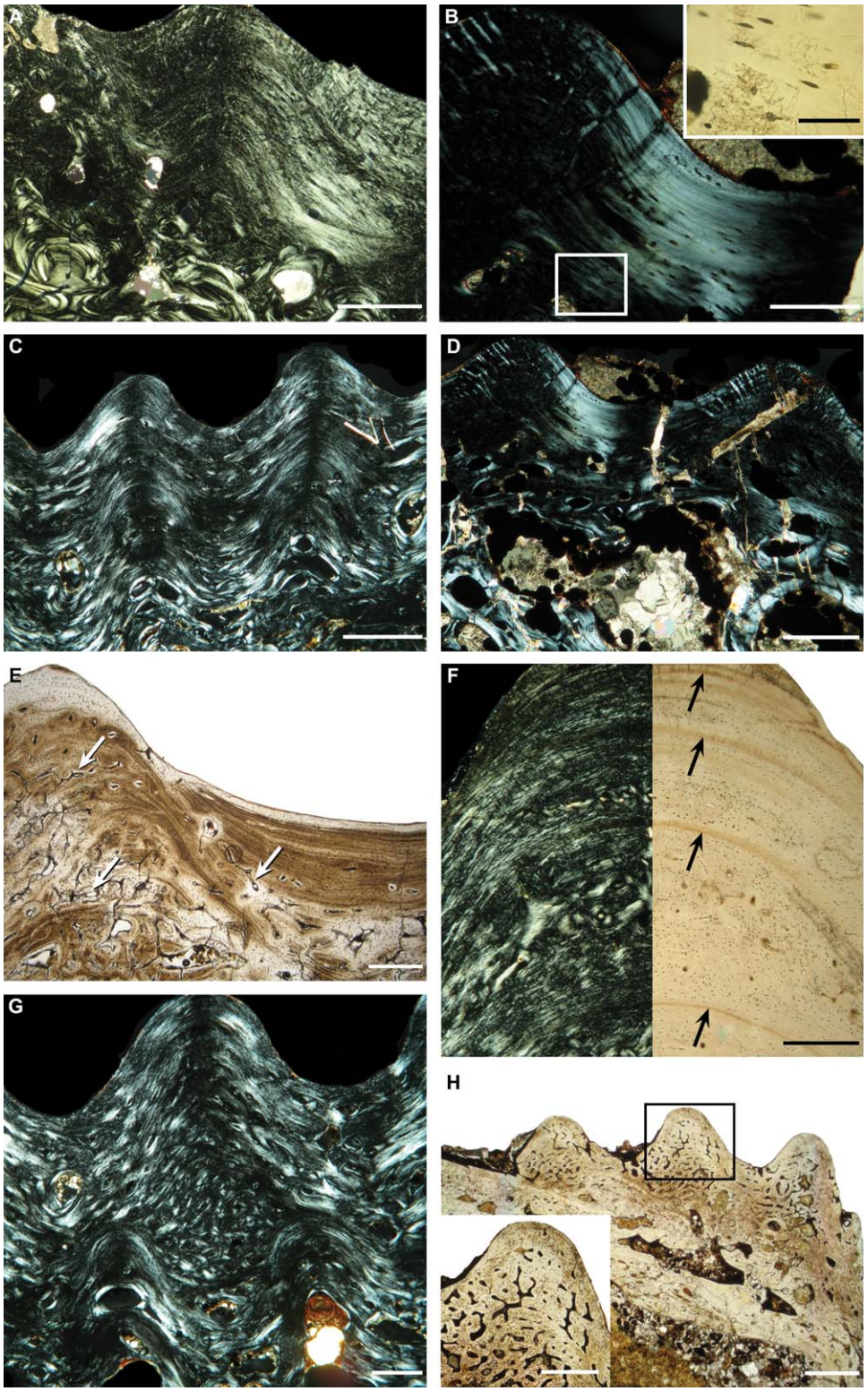

Fig. 3. Histological features of the superficial cortex in the temnospondyls, and in *Diplocaulus* and *Bystrowiana* ornamented bones. **A**: Parallel-fibered bone of variable birefringence in the skull bone of *Platyoposaurus* (polarized light). **B**: Parallel-fibered bone of variable birefringence in an undetermined skull bone of a Late Permian *Diplocaulus* (polarized light). The insert shows the difference in the morphology of cell lacunae between the woven-fibered-like tissue occupying the core of the bone, and the parallel-fibered tissue located in the floor of the pits. **C**: Skull bone of a Middle Triassic *Stanocephalosaurus* (polarized light). Bone deposits are regular and continuous, with no reversion line, from the depth up to the surface of the cortex. **D**: Skull bone of *Diplocaulus* (polarized light). The cores of the ridges are quasi-monorefringent. **E**: Skull bone of *Stanocephalosaurus*. Vascular canals (arrows) occur in the ridge and, to a lesser extent, in the floor of the pit. **F**: Histology of a ridge in a Middle Triassic *Kupferzellia* postparietal. Left half: polarized light; right half: natural, transmitted light. Vascular canals are unevenly distributed, according to the conspicuous cyclical growth marks (arrows). **G**: Vascular proliferation at the base of a ridge, just above a filled pit, in *Stanocephalosaurus* (polarized transmitted light). H: Unusual tissue displaying reticular vascularization (framed field and insert) in the ornamented cortex of a skull bone from the Late Triassic *Benthosuchus sushkini*. Scale bars: C, H = 1 mm; A, D, E-G, H insert = 500 μm; B main frame = 200 μm; B insert = 50 μm.

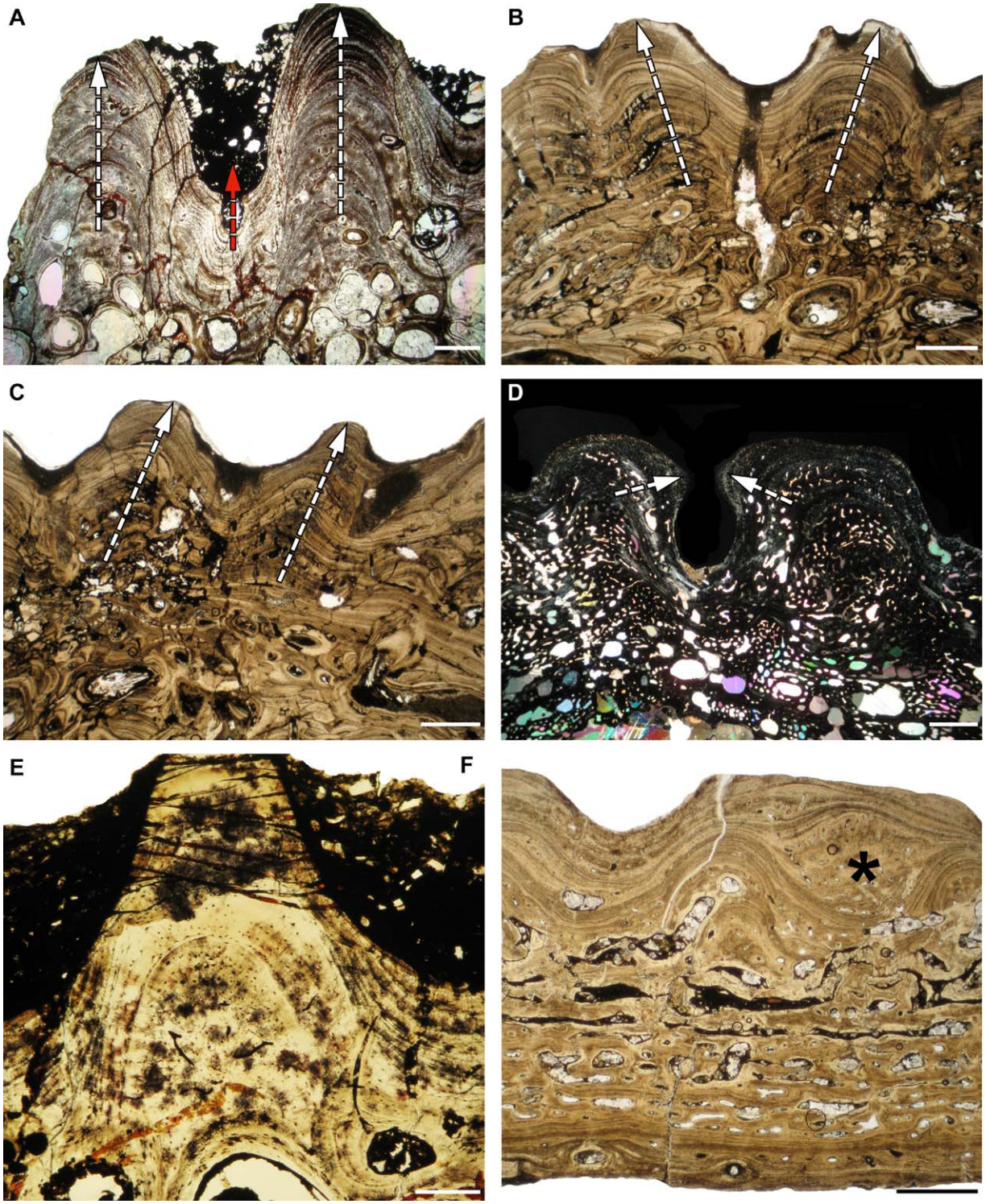

Fig. 4. Dynamic processes in the ornamented cortices of temnospondyls. **A**: Straight, simple centered piling growth of the ridges of the interclavicle of the Late Triassic *Dutuitosaurus*. The pit remains narrow and its depth increases. The dashed arrows indicate the direction of growth over the ridges (white arrows) and pit floor (red arrow). **B**: Symmetric divergence of the ridges during growth. Skull bone of the Early Permian *Eryops megacephalus*. Same symbols as for A. **C**: Sub-parallel ridge drift in the bone of *Eryops megacephalus*. **D**: Convergent ridge drift in the postparietal of the Middle Triassic *Plagiosuchus* (polarized light). **E**: Decrease in ridge width during growth in a Late Permian *Peltobatrachus* osteoderm. **F**: Pit filling (asterisk) in the interclavicle of *Plagiosternum*. Scale bars: A-D, F = 1 mm; E = 250 μm.

narrowing. This situation is frequent (if not general), and was observed in all specimens, except *Benthosuchus*, *Diplocaulus*, *Plagiosuchus*, and one of the *Stanocephalosaurus* specimens.

4. Convergent ridge drift (Fig. 4D). In this case, the ridges surrounding a pit present off-centered periosteal accretion, but this process occurs centripetally toward pit central axis, thus provoking a gradual narrowing of pit diameter, and creating a trend toward local pit closure. This rare process was observed only in the postparietal of *Plagiosuchus*.
5. Reduction of ridge width (Fig. 4E). Periosteal bone accretion can be much faster on the tip of a ridge than on its lateral sides. This process results in a fast increase in ridge height, accompanied with a relative decrease of ridge width (Fig. 4E). Ridges then tend to become sharper during growth and the pits that they border turn proportionally wider and deeper. This rare case was mainly observed in *Peltobatrachus*.
6. Pit filling and relief inversion (Figs. 3G, 4F). Pits can be entirely filled, and disappear to be replaced in situ by ridges. This process relies on a steep acceleration of bone accretion on pit floor, as typically evidenced on bone sections by a local increase in the spatial density of vascular canals (e.g., Fig. 3G). Growth acceleration proceeds until a protruding relief, which actually represents the base of a newly formed ridge, is created. The ridge is then submitted to one or several of the five other morphogenetic processes described above. This relief inversion is relatively frequent; it was observed in *Dutuitosaurus*, *Mastodonsaurus*, *Plagiosternum* and *Stanocephalosaurus*.

Embolomeri (*Archeria*).

General histological features. The bone of *Archeria* examined here is a diploe of medium compactness (88.7%), with avascular and compact cortices (Fig. 5A). The very intense remodeling activity that occurred in the core region of the bone (Fig. 5B) left only scarce remnants of primary bone tissue. The latter has the same gross histological structure as the superficial, ornamented layer that actually represents its upward extension. The superficial layer is composed of a tissue close to the parallel-fibered type, exhibiting poor birefringence in the ridges, and brighter birefringence in the layers forming the floor of the pits (Fig. 5C). Osteocyte lacunae have a rounded shape, an aspect possibly due to their orientation relative to the section plane (their true morphology might thus be spindle-like). This tissue is integrally subdivided into parallel layers by cyclic growth marks, represented by lines of arrested growth, or LAGs (Fig. 5D). All of them are split (they appear as double lines), suggesting that the animal's ecology was characterized by a short period of activity resumption between two yearly diapause phases. The superficial layer is devoid of any sign of resorption or remodeling, and is in mere continuation with the deeper osseous strata located in the core of the bone; however the spacing of the LAGs is wide in the ridges, and narrower in the floor of the pits, thus indicating pronounced differences in local growth rates (Fig. 5D). The basal layer of the bone is made of an avascular, lamellar bone tissue displaying short bundles of Sharpey's fibers, but where cyclic growth marks do not occur (Fig. 5C).

Interpretation of growth patterns. Since parallel-fibered bone tissue is considered to result from faster accretion than lamellar tissue (Castanet et al., 1996, 2000; Margerie et al., 2002, 2004; see also Francillon-Vieillot et al., 1990; Ricqlès et al., 1991), bone growth must have been more active over the ornamented surface than over the basal cortex. The differences observed in both the refringence properties of the bone and the spacing of the LAGs suggest that the ornamental reliefs were produced, as in the temnospondyls, by local contrasts in growth rates between the top of the ridges (fast accretion) and the bottom of the pits (slow accretion). Ridge growth involved no significant drift that could have resulted in pit widening, displacing or entire filling. Pit widening thus appears to have been dependent on a single possible (though not evidenced on the sections) mechanism during growth: a decrease in ridge width.

Lissamphibia (*Ceratophrys*, *Latonia*, and *Thaumastosaurus*).

General histological features. The microanatomical organization of *Ceratophrys* and, to a lesser extent, *Latonia* fronto-parietals is that of a typical diploe, with highly compact cortices framing a loose, central spongiosa (Fig. 6A). The fronto-parietal of *Thaumastosaurus*, like the maxillaries of the three taxa, does not have a diploe structure, although broad resorption bays occur in their central region. Bone tissue in our *Thaumastosaurus* specimen is too degraded to allow detailed observations. In the other two taxa, the most central region of the bones displays a thin (some 50–60μm in maximal thickness in *Ceratophrys*; 70-90 μm in *Latonia*) layer of a monorefringent tissue (Fig. 6A,B) whose general characteristics (morphology and spatial density of cell lacunae: Fig. 6C,D) correspond to the woven-fibered tissue type. This bone layer contains few simple vascular canals (Fig. 6B,D), but these have a wide lumen (up to 50 μm) because of the resorption, followed or not by partial, secondary reconstruction, which occurs on their walls. The deep (basal) cortices are avascular, nonremodeled, and made of parallel-fibered tissue (mass birefringence, spindle-like cell lacunae oriented parallel to bone layers: Fig. 6A,B).

In *Ceratophrys*, the superficial, ornamented cortex has a complex histological structure. Its deep part, in contact with the woven-fibered layer, consists of typical parallel-fibered tissue housing wide

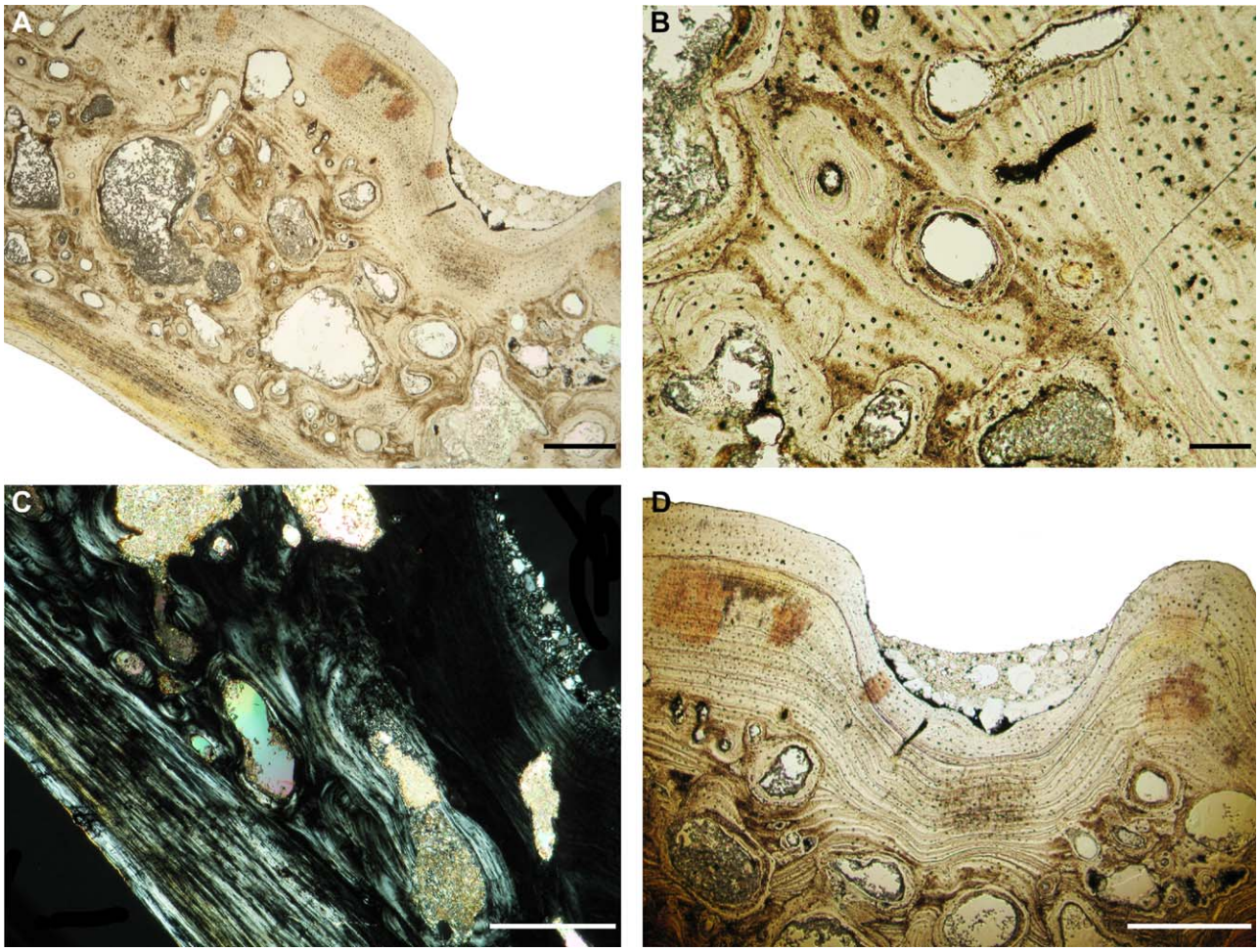

Fig. 5. General histology of ornamented bones in *Archeria*. **A**: General view of the diploe architecture of an Early Permian *Archeria* bone. **B**: Closer view at the intensely remodeled tissue forming the core of the same *Archeria* bone. **C**: Aspect of the basal and superficial cortices of the same *Archeria* bone (polarized light). The basal cortex is made of lamellar tissue, whereas the superficial cortex is of a parallel-fibered type, more birefringent in the floor of the pits than in the core of the ridges. **D**: Cyclical growth marks in the superficial cortex of the same *Archeria* bone. Marks are more tightly spaced in the pit floor. There is no discontinuity or reversion line between the superficial, ornamented layer and the subjacent, remodeled tissue located in the core of the bone. Scale bars: A, C, D = 500 μm; B = 100 μm.

vascular canals that may locally turn into broad erosion bays (Fig. 6C–E). The ornamentation ridges situated upon this layer can display two very distinct patterns in their histological structure: a few are made of the same parallel-fibered tissue as observed in the subjacent layer, of which they merely represent a superficial excrescence displaying signs of inner remodeling (Fig. 6E). However, most of the ridges are made of an avascular tissue that shows a very conspicuous and regular stratification appearing in polarized light in the form of alternatively bright and dark strata of even thickness (Fig. 6C,F,G). Considering the individual thickness of the strata (8–12 μm for the dark ones; 7–8 μm for the light ones), this tissue is unlikely to be true lamellar bone because the thickness of bone lamellae (from 2 to 6 μm, at most) seldom exceeds 5 μm (Currey, 2002); moreover, the regularity of the strata (as also their position within the cortex: see below) precludes the possibility that they represent yearly growth marks. This stratified layer rather represents a peculiar tissue undescribed hitherto in the skull bones of lissamphibians. Its pattern is strongly reminiscent of the "plywood-like structure" described in the carapace of the Trionychidae (soft-shelled turtles) by Scheyer et al. (2007, 2012), and it will tentatively be referred to this tissue, though it lacks the "vertically oriented plies" exhibited by the turtle bones (see also below: "Testudines"). Interestingly, a similar tissue (with slightly thicker lamellae of about 15–18 μm) has also been mentioned in the osteoderms of the Dissorophidae (in *Aspidosaurus* and *Platyhystrix*), a Permian temnospondyl taxon from which several (but not all) authors think that lissamphibians arose (Witzmann and Soler-Gijón, 2010). In *Ceratophrys*, the stratified, plywood-like tissue can be covered, on the apex of the ridges, by a layer of avascular poorly birefringent

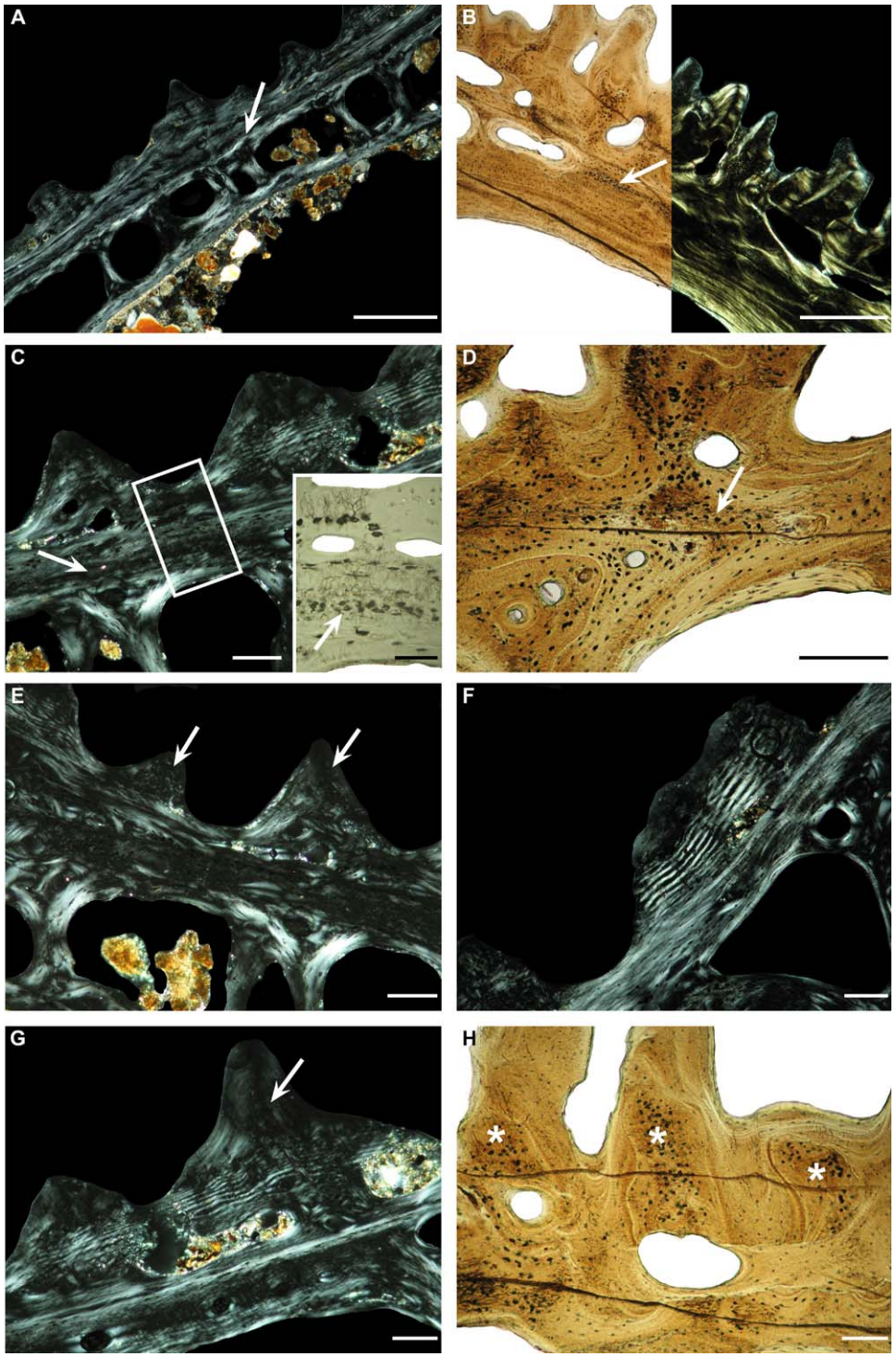

Fig. 6. General histology of ornamented bones in lissamphibians (extant, unless specified otherwise). **A**: Cross section in the fronto-parietal of *Ceratophrys* (polarized light). The general structure is that of a diploe. The arrow points to the thin sheet of monorefringent tissue in the center of the bone. **B**: Cross section in the fronto-parietal of the mid-Miocene *Latonia gigantea* (left half: natural transmitted light; right half: transmitted polarized light). Same symbol as for part A. **C**: Closer view at the central monorefringent bone layer (arrow) in *Ceratophrys* (main frame: polarized light; insert: natural light). **D**: Closer view at the central monorefringent tissue (arrow) in the maxillary of *Latonia*. **E**: Ornamented layer in *Ceratophrys* frontoparietal, with ridges made of remodeled parallel-fibered tissue (arrow) (polarized light). **F**: Superficial layer of plywood-like tissue in the fronto-parietal of *Ceratophrys* (polarized light). **G**: Other view at the plywood-like superficial tissue in the ridges of *Ceratophrys* frontoparietal (polarized light). The apex of the ridge is capped by a poorly-birefringent parallel-fibered tissue with few cell lacunae (arrows). **H**: Ridge structure in *Latonia* fronto-parietal. Deep woven-fibered tissue (asterisks) protrudes into the core of the ridges. Scale bars: A, B = 500 μm; D = 200 μm; C main frame, E-H = 100 μm; C insert = 50 μm.

parallel-fibered bone containing few cell lacunae (Fig. 6A,C,F,G).

In *Latonia*, the superficial, ornamented cortex is basically made of a brightly birefringent and intensely remodeled, parallel-fibered tissue (Fig. 6B,H). However, the core of the ridges comprises an excrescence of the subjacent woven-fibered layer (Fig. 6D,H).

In the three lissamphibian taxa, the superficial, ornamented cortex shows obvious signs of an intense remodeling activity in the form of extensive resorption (unambiguously evidenced by Howship's lacunae; cf. Fig. 7A), followed by partial reconstruction. In *Ceratophrys*, the resorption extends to the whole superficial cortex, though it is actually subdivided into punctual spots (Figs. 6A and 7A,B). It tends to erode both the layer of primary stratified tissue, in which it excavates very sharp and clear-cut pits (e.g., Figs. 6F,G, and 7B), and the subjacent parallel-fibered layer (Fig. 7A–C). The subsequent phase of partial reconstruction (that can itself be followed by a new resorption phase: Fig. 7F,G) sets thin layers of lamellar bone on the bottom and walls of the pits. These reconstructive deposits often show the same asymmetry between the medial and lateral sides of the ridges (e.g., Fig. 7D,F,H) as that previously described in crocodilians by Buffrénil et al. (2015). In *Ceratophrys*, there is apparently no other mechanism for the differentiation of ornamental reliefs than the double process of extensive (but patchy), superficial resorption and partial reconstruction. The same mechanism is likely to have occurred also in *Thaumastosaurus* because ornamented cortices in this taxon show a similar remodeling pattern as that observed in *Ceratophrys* bones (Fig. 7D). In *Latonia*, the situation might have been more complex. The excrescences of woven-fibered bone that protrude in the core of the ridges suggest that the initial stage of ridge differentiation in this taxon was a local and temporary acceleration of bone accretion. Subsequently, an intense remodeling activity involving several resorption and reconstruction cycles occurred on cortical surface (Fig. 7E–G). It was topographically related to the course of the vascular canals running inside the bones, and their outcrop on the bone surface in the middle of pit floors (Fig. 7F,G,I). This remodeling process resulted in a steep deepening of the pits, whose bottoms were reconstructed but very partially. Such a remodeling pattern is fairly different from that observed in *Ceratophrys* and *Thaumastosaurus*, and created a distinct morphology of bone ornamentation: tall, columnar ridges framing deep and narrow well-like pits. In addition, off-centering and topographic drift processes occurred during crest growth in the fronto-parietal and maxillaries of *Thaumastosaurus* (Fig. 7H) and *Latonia* (Fig. 7I).

Amniota

Captorhinidae (*Captorhinus aguti*).

General histological features. The skull roof fragment of *Captorhinus aguti* has a classical diploe architecture (compactness 91.3%). All the cavities located in the core of the bone are former erosion bays whose walls were partly reconstructed by secondary, endosteal deposits of lamellar tissue (Fig. 8A). Between these cavities, abundant remnants of the primary bone deposited at early growth stages remain visible. In polarized transmitted light, this tissue shows a poor and irregular, though detectable, birefringence (Fig. 8B). Local osteocyte lacunae have abundant canaliculi, and a spheroid, multipolar or spindle-like shape; this morphological variability is indicative of their uneven orientation within the bone matrix (Fig. 8B, insert). Considered together, these histological traits suggest the occurrence of a woven-fibered bone tissue type with an atypical intercellular matrix turning into the parallel-fibered type (incipient birefringence). Local vascularization is mainly composed of primary osteons (lumen 25–40 μm in diameter), though few simple vascular canals 10–18 μm in diameter may occur in some areas. The basal cortex of the bone is composed of primary bone tissue (remodeling is very limited) displaying histological features similar to those of the core region. However, in the basal region, birefringence is more pronounced, and vascular canals are mainly simple canals.

The tissue forming the core of the bone extends with no significant modification toward the ornamented, superficial layer, where it constitutes most of the volume of the ridges (Fig. 8C). The outermost ridge strata, over a thickness of some 50–60 μm, as well as the thicker (100–120 μm) bone layer forming the bottom of the pits, are composed of a brightly birefringent parallel-fibered tissue with flat cell lacunae oriented parallel to the general direction of bone layers (Fig. 8C,D). This layer is avascular but may display Sharpey's fibers as dense bundles perpendicular to the surface of the bone. The *Captorhinus* bone examined here displays no cyclic growth marks.

Dynamic processes in superficial cortices. Histological evidence clearly rules out any involvement of superficial remodeling in the development of bone ornamentation in *Captorhinus*. The osseous tissue occurring in ridges is basically similar in structure to that located in the core of the bone, and differs very little from the tissue forming the basal layer. Considering the general, well-established, relationships between bone structure and appositional rate, as reviewed above (cf. chapter "material and methods"), ridges are unlikely to have resulted from local acceleration of periosteal accretion. Conversely, the parallel-fibered bone located on the bottom and walls of the pits is known to grow more slowly than the woven-fibered-like tissue in the ridges. The differentiation of bone sculpture would thus result

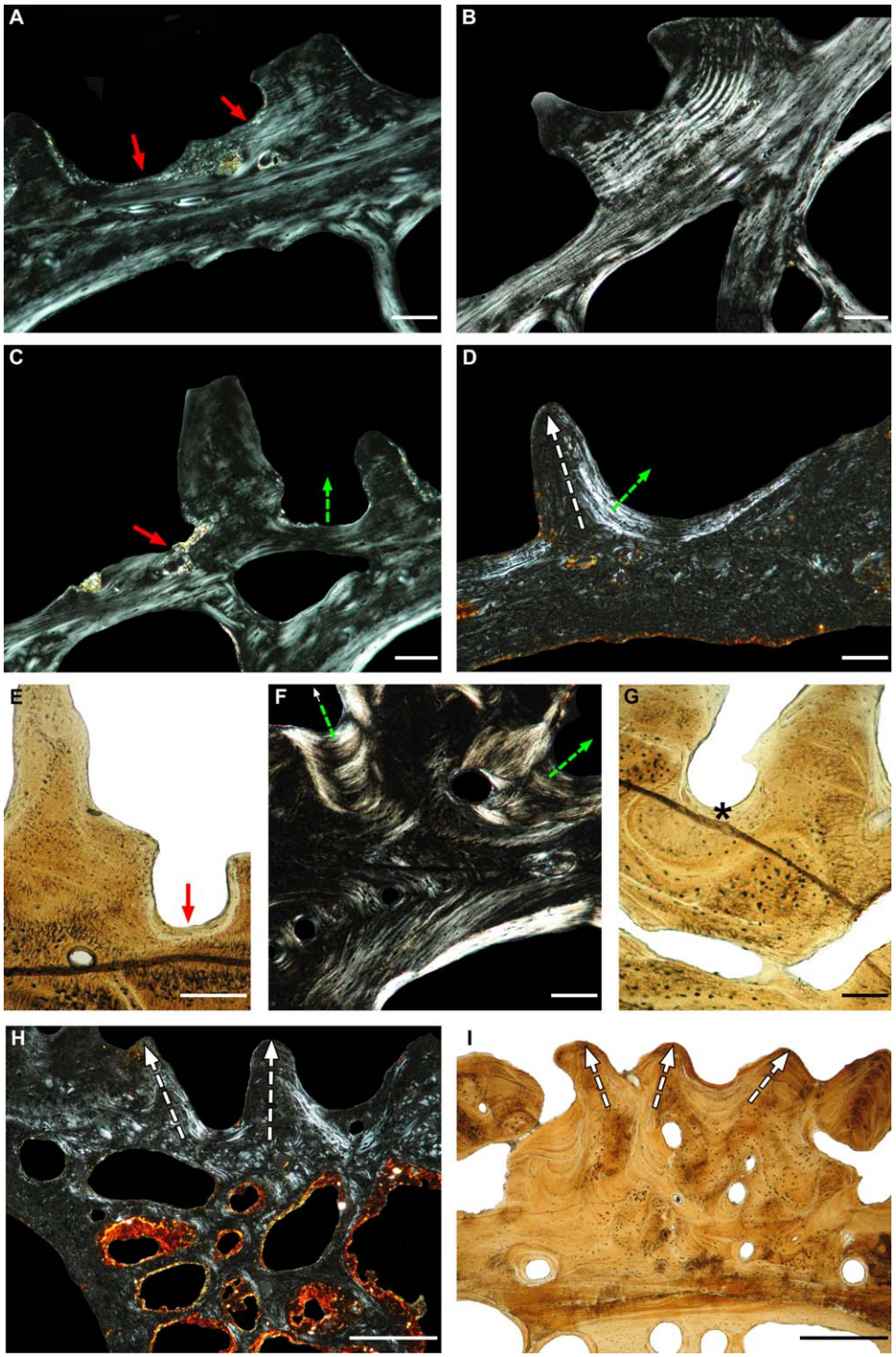

Fig. 7. Remodeling of the ornamented layer in lissamphibians (taxa are extant, unless specified otherwise). **A**: Active resorption (red arrows) in the frontoparietal of *Ceratophrys* (polarized light). **B**: Detail of the clear-cut resorption of the superficial plywood-like layer in the frontoparietal of *Ceratophrys* (polarized light). **C**: Intense resorption process (red arrow) reaching the deep layers of the cortex in *Ceratophrys* frontoparietal (polarized light). The floor of the next pit is under reconstruction (green dashed arrow) (polarized light). **D**: Asymmetric resorption and reconstruction (green dashed arrow) on the frontoparietal of the Eocene *Thaumastosaurus* (polarized light). **E**: Local resorption (red arrow) in the frontoparietal of the mid-Miocene *Latonia*. **F**: Remodeling through asymmetric resorption and reconstruction (arrows) in the frontoparietal of *Latonia* (polarized light). **G**: Remodeling in the vicinity of vascular canals (asterisk) that outcrop on pit floor in *Latonia* frontoparietal. H: Lateral ridge drift (dashed arrows) in the frontoparietal of *Thaumastosaurus* (polarized light). **I**: Divergent and lateral ridge drifts (dashed arrows) in the maxillary of *Latonia*. Scale bars: H, I = 500 μm; E = 200 μm; A–D, F, G = 100 μm.

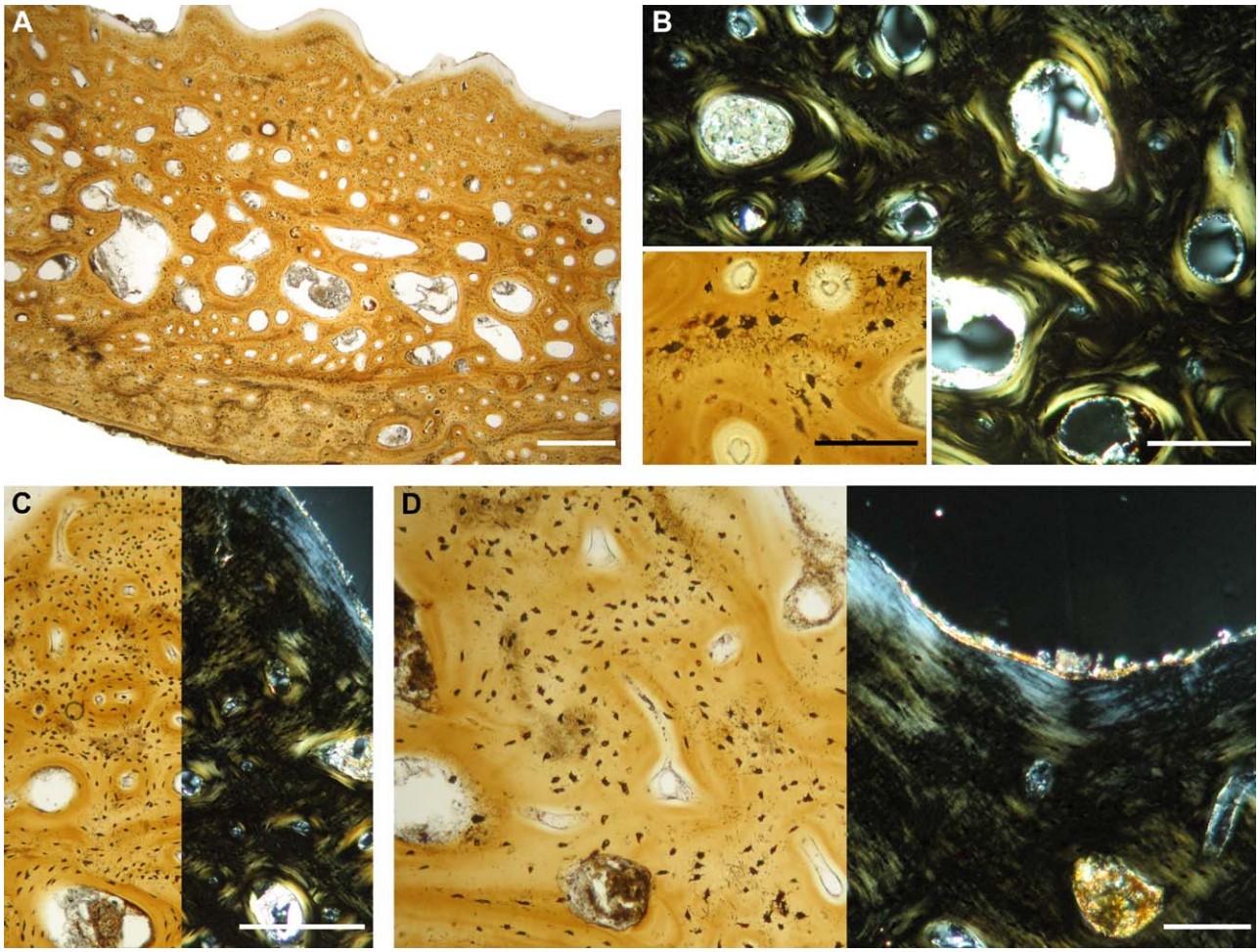

Fig. 8. General histology of ornamented bones in *Captorhinus*. **A**: General diploe-like architecture of an Early Permian *Captorhinus* bone. **B**: Poor birefringence of the remodeled tissue located in the core of that bone (polarized light). The insert shows the multipolar cell lacunae enclosed in the remnants of primary tissue that persist between secondary osteons. **C**: Tissue forming the bulk of the ridges (left half: natural transmitted light; right half: transmitted polarized light). **D**: Birefringent layer covering the sides of ridges and the bottom of pits in the superficial cortex (left half: natural transmitted light; right half: transmitted polarized light). Scale bars: A = 500 μm; C = 250 μm; B main fame, D = 100 μm; B insert = 50 μm.

from the simple mechanism also encountered in temnospondyls and *Archeria*: a discrepancy in accretion rate between the bottom of the pits, where growth was slow, and the top of the ridges, where growth proceeded at the same rate as that occurring on the other parts of the bone surface (except pit bottom and walls). Pit differentiation would have resulted from this local contrast in growth rates. Moreover, there is no indication of spatial drift or off-centering in ridge growth. This general growth pattern offers few possibilities for pit enlargement during growth, with exception for the "decrease in ridge width" mentioned above.

Testudines (Trionychidae, Emydidae, Araripemidae).

General histological features. Ornamented bones in the six chelonian taxa studied here have a typical diploe structure, but strong differences in bone compactness exist between samples (from 82.9% in *Trionyx triunguis* to 96.4% in *Araripemys barretoi*). The basic traits of their histological structure are also comparable (Fig. 9A): their basal cortex consists of a homogeneous and brightly birefringent layer of parallel-fibered tissue that turns, toward the bone periphery, into lamellar tissue. Local vascularization, represented by scarce simple vascular canals, is uneven between taxa. The core of the bones is occupied by monorefringent woven-fibered tissue displaying thick, randomly oriented fiber bundles (i.e. the "interwoven-structural collagenous fiber bundles" of Scheyer and Sánchez-Villagra, 2007) (Fig. 9A, left insert). This region is submitted to intense remodeling through which the deep, compact strata of the cortex are progressively made cancellous (Fig. 9A, right insert). The superficial, ornamented cortex is a thick layer of variably birefringent parallel-fibered tissue. The parts of this layer forming the floor of the pits are always more birefringent, and closer to the lamellar tissue type, than those forming the

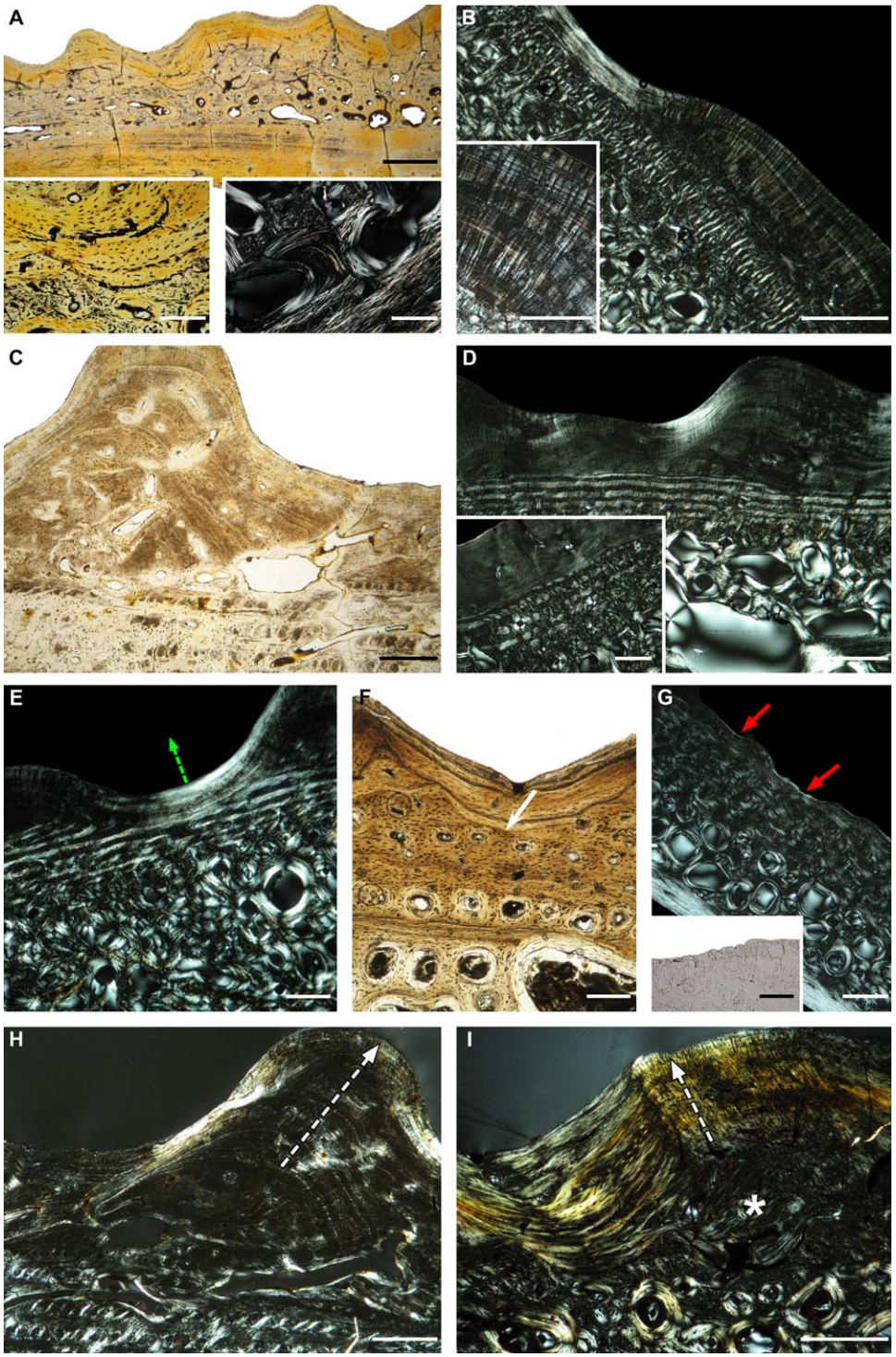

Fig. 9. Histology of carapace plates in Testudines. **A**: General histology of a carapace plate of the Early Cretaceous *Araripemys*. The left insert shows the difference between the woven-fibered tissue located in the core of the plates, and the parallel-fibered cortices. The insert on the right shows the intense remodeling of the core region (polarized light). **B**: Parallel-fibered tissue in the superficial cortex of the extant *Trionyx triunguis*. Abundant bundles of Sharpey's fibers located preferentially within the ridges cross the cortex (main frame and insert in polarized light). **C**: Annuli and simple vascular canals in the superficial cortex of a Late Cretaceous *Aspideretoides* carapace plate. **D**: Plywood-like bone layer encountered in the carapace of the extant trionychids (main frame and insert in polarized light). **E**: Resorption and subsequent reconstruction (green dashed arrow) of the superficial cortex in the extant *Amyda cartilaginea* (polarized light). **F**: Wavy contour of the resorption line (arrow) that marks the limit of a former resorption field in *Araripemys*. **G**: Howship's lacunae (red arrows) on bone surface in the extant *Pseudemys* (main frame: polarized light; insert: Howship's lacunae viewed in ordinary transmitted light). **H**: Lateral ridge drift (dashed arrow) in *Aspideretoides* (polarized light). **I**: Ridge drift (dashed arrow) with multiple resorption/reconstruction cycles, along with pit filling (asterisk) in *Araripemys* (polarized light). Scale bars: A main frame = 1 mm; B main frame, C, D main frame, G-I = 500 μm; A inserts, B insert, D insert, E, F = 250 μm; G insert = 50 μm.

ridges (Fig. 9B). Abundant, vertically oriented bundles of Sharpey's fibers cross the whole thickness of the superficial layer, with a characteristic discrepancy between the pits that have few or no fiber bundles, and the ridges in which most of the fiber bundles occur (Fig. 9B). Like the basal cortex, the superficial, ornamented layer may, or may not, display simple vascular canals and cyclical growth marks in the form of annuli (Fig. 9B,C). The main difference between taxa is the occurrence or the absence of a plywood-like bone layer (a tissue described by Scheyer et al., 2007, 2012; see also Landmann, 1986) consisting of alternatively birefringent and monorefringent strata (an aspect due to the orthogonal orientation of fibers between adjacent strata), linked by strong vertical fiber piles (Fig. 9D–E). This layer is located just under the parallel-fibered bone that bears ornamentation, and occurs exclusively in the trionychids (here: *Amyda cartilaginea*, *Cyclanorbis sp*., *Trionyx triunguis*, and *Aspideretoides*), as already mentioned by Scheyer et al. (2007).

Remodeling of the ornamented layer. In all the specimens examined here (be they trionychids, or araripemyds), except the emydid *Pseudemys*, the superficial, ornamented layer is separated from the subjacent bone strata (woven-fibered bone or plywood-like layer) by a reversion line, with discordant bone deposits above and under this line (Fig. 9D–F,I). Bone deposits situated above the line are thus secondary, reconstructive deposits that can extend continuously over the whole bone surface, or be interrupted by outcrops of the subjacent primary tissue, set to surface by the resorption process. The reversion line is often straight in a part of its course (Fig. 9D) and wavy in other parts, according to the local contour of bone ornamentation (Fig. 9E,F). There is no resorption line in the superficial cortex of the *Pseudemys* specimen examined here. However, in several spots corresponding to the floor of shallow pits, the surface of the bone displays slight depressions bordered by well-characterized Howship's lacunae (Fig. 9G) that unambiguously indicate that a superficial resorption process was active by the time the animal died. This apparent exception finally confirms the general pattern observed in the other taxa. Histological sections also reveal that bone ornamentation in the Testudines experiences the same processes of lateral ridge drift (Fig. 9C,H) or pit filling (Fig. 9I) as those observed in most other taxa described above.

Histological observations suggest that the mode of formation of bone ornamentation on turtle carapace plates relies on osteogenic processes reminiscent of those previously observed in crocodilians (Buffrénil et al., 2015), or described above about lissamphibians. The main peculiarity that distinguishes the turtles from these taxa is the occurrence of an extensive resorption field able to level the preexisting surface of the bone before the accretion of the ornamented surface. According to the local contour, straight or sinuous, of the resorption line, two slightly distinct modalities for the development of bone ornamentation can take place: 1) Local bone surface has been made flat by resorption; ornamental reliefs would then result from slight differences in bone accretion rates between the top of the ridges (faster growth forming poorly birefringent parallel-fibered tissue), and the floor of the pits (slower growth forming a tissue between the parallel-fibered and the lamellar types). This case is illustrated on Fig. 9D. 2) Resorption did not flatten entirely the surface of the bone; then, subsequent accretion of future bone layers further enhances the preexisting reliefs (illustrated on Fig. 9F). In all cases, the development of the ridges seems to be topographically related to, and perhaps facilitated by, the insertion of particularly strong Sharpey's fiber bundles into the bone cortex, a hypothesis already considered by Witzmann (2009) for early stegocephalians. During further growth, the control of pit depth and diameter mainly relies on symmetric or asymmetric ridge drift. Multiple resorption and reconstruction cycles, similar to those described above in the lissamphibians (and general in the pseudosuchians: Buffrénil et al., 2015), are seldom observed in the turtles; however, they may nevertheless occur, as exemplified by the carapace plate of *Araripemys* (Fig. 9I).

Squamata (*Necrosaurus*).

General histology. Though the two necrosaur osteoderms are different in morphology (one has a strong median keel, while the other is nearly flat), they show similar microanatomical and histological organizations, though one of them is more compact than the other (93.7% vs 82%), but contain broad, central cavities due to resorption (occurrence of Howship's lacunae), whose walls are partly reconstructed by endosteal, lamellar deposits (Fig. 10A–C). The core of each osteoderm is occupied by a monorefringent tissue that nevertheless displays numerous thick birefringent fiber bundles (Fig. 10C). Local osteocyte lacunae are ovoid or multipolar with few canaliculi. This tissue can be classified as a form of woven-fibered bone tissue. It is covered on its superficial and basal sides by thick layers of brightly birefringent parallel-fibered bone (Fig. 10A–D) containing Sharpey's fibers. These layers are histologically homogenous, and display only a faint indication of cyclic growth (Fig. 10D). The superficial, ornamented layer lacks any obvious sign of local acceleration or deceleration of growth. It lays in continuity with the subjacent monorefringent tissue, and no reversion line delimits these two tissues. In the design of its inner stratification, as also in its surface reliefs, the ornamented layer, especially that of the keeled osteoderm, follows slight undulations already displayed by the monorefringent tissue over which it develops. Moreover, the bottom of the ornamental pits exhibits clear evidence of bone resorption, in the form of Howship's lacunae (Fig. 10D). This process is

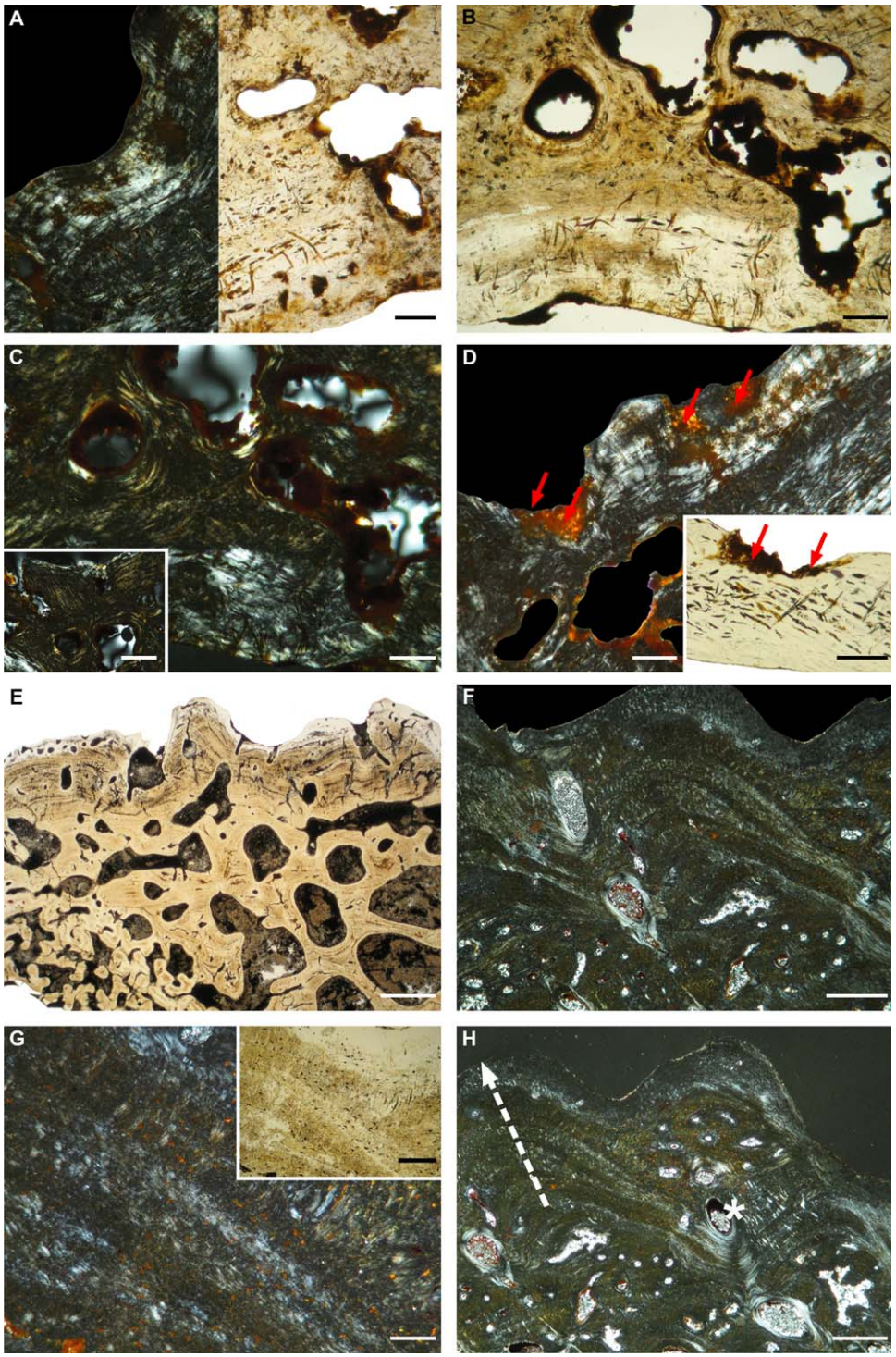

Fig. 10. General histology of ornamented bones in *Necrosaurus* and *Lupeosaurus*. **A**: General structure of an Eocene *Necrosaurus* osteoderm, with birefringent superficial and basal cortices framing a monorefringent core (left half: polarized light; right half: normal light). **B**: Broad central cavities in a *Necrosaurus* osteoderm. **C**: Tissue akin to woven-fibered bone in the core of a *Necrosaurus* osteoderm, with a small part of the subjacent birefringent basal cortex. The insert shows the abundant Sharpey's fibers in the basal cortex (main frame and insert in polarized light). **D**: Superficial resorption (red arrows) not followed by reconstruction in a *Necrosaurus* osteoderm (main frame: polarized light). **E**: General view of an Early Permian *Lupeosaurus* bone. **F**: Avascular cortex made of a poorly birefringent parallel-fibered-like tissue in the bone of *Lupeosaurus*. This bone displays broad annuli that tend to fuse with each other in the floors of the pits (polarized light). **G**: Detail of the histological structure of the tissue forming the ridges. The insert shows that osteocyte lacunae show great differences in canaliculi development between dark, opaque layers and translucent layers (main frame: polarized light). **H**: Lateral ridge drift (white dashed arrow) and pit filling (asterisk) in the ornamented cortex of *Lupeosaurus* bone (polarized light). Scale bars: E = 1 mm; F, H = 500 μm; C insert = 200 μm; G insert = 150 μm; A-D, G main frame = 100 μm.

topographically related to the course of large inner vascular canals whose superficial outcrops were widened by the local resorption. In no case was resorption followed by reconstruction.

Growth pattern of the osteoderm and its ornamentation. In reference to data available about the development of squamate osteoderms (e.g., Buffrénil et al., 2011), the histological observations presented above suggest that necrosaur osteoderms were produced by a double osteogenic process: i) initial dermo-osseous metaplasia that created the woven-fibered tissue of the core region; ii) later in ontogeny, typical osteoblastic accretion of bone that produced the outer, parallel-fibered birefringent layers. The former occurrence of osteoblasts around the osteoderm is evidenced by the endosteal deposits covering the walls of inner cavities: endosteal osteoblasts are known to derive from periosteal osteoblasts that penetrate the core of a bone along its vascular canals (Krstic, 1985; Karaplis, 2008). Ornamentation pits seem to have resulted from a double process. For a limited part (and especially in the keeled osteoderm), they were the mere repercussion on the surface of deeper reliefs borne by the bone forming the core of the osteoderms. For another part, they resulted from an increase of these faint initial reliefs through local resorption in the vicinity of vascular pits. This additional process is likely to have occurred at a relatively late stage of osteoderm growth, when the superficial layer had reached an advanced stage of development. No reconstructive phase, and thus no remodeling in the proper sense, was involved.

Synapsida: Edaphosauridae (*Lupeosaurus*).

General histological features. The *Lupeosaurus* bone fragment is not truly organized as a diploe. It displays a few broad, sub-circular central cavities surrounded by numerous smaller, partly reconstructed resorption bays that colonize also the basal cortex (Fig. 10E). The superficial, ornamented cortex is compact with few, small-diameter primary osteons and simple vascular canals (Fig. 10E,F), along with thick bundles of Sharpey's fibers. Primary bone deposits, be they located in the core of the bone or in the superficial and basal cortices, are characterized by the succession of thick bone layers (thickness of 150–200 μm), alternatively monorefringent with high opacity, and birefringent with low opacity (Fig. 10F,G). Differences in opacity between the layers result from discrepancies in the density of the osteocyte lacunae (less numerous in the light layers), the morphology of their soma, and the abundance of their canaliculi, particularly well-developed in the darker layers (Fig. 10G). This histological structure is indicative of a cyclic growth, with the darker layers featuring "zones" laid down during episodes of fast growth, and the lighter layers representing *annuli*, formed during phases of slower growth. The superficial layer displays neither reversion lines separating discordant bone layers, nor any trace of superficial bone resorption or remodeling.

The spacing of the cyclic growth marks indicates higher growth rates at the level of the ridges than in the pits (Fig. 10F,H): pit floor is made of tightly packed annuli, with nearly no zone inserted between them. Therefore, the differentiation of bone ornamentation in *Lupeosaurus* was mainly a result of local differences in accretion rate, as it was observed above in many other taxa. Moreover, the development of bone ornamentation during growth in *Lupeosaurus* was submitted to the same dynamic trends as those described in the temnospondyls: total ridge drift (Fig. 10F,H), pit filling, and inversion of local reliefs (a ridge replacing a pit: Fig. 10H). In the latter case, the characteristic increase in bone vascularization at the base of the new ridge that was observed in several other taxa, such as the temnospondyls *Stanocephalosaurus* (cf. Fig. 3G) or *Plagiosternum* (Fig. 4F), also occurs in *Lupeosaurus*.

Actinopterygii

Acipenseriformes (*Acipenser sturio*). The opercular of *Acipenser sturio* is not a diploe; it is formed by the junction of two compact cortices: the basal one has a smooth surface; the superficial one displays deep well-like pits separated by vertical ridges (Fig. 11A). Both cortices are made of parallel-fibered bone. This tissue is less brightly birefringent in the superficial cortex than in the basal one. Birefringence is particularly faint in the core of the ridges; conversely, ridge sides are made of strongly birefringent lamellar bone (Fig. 11B). Cell lacunae are typical of parallel-fibered bone (they are flat, without canaliculi) except in the core of the ridges, where they show a multipolar shape and long canaliculi forming a dense network (Fig. 11C,D). Between the two cortices, a thin (thickness 70–120 μm) discontinuous blade of a more opaque tissue displaying multipolar cell lacunae with canaliculi appears locally. The opercular of *Acipenser* is avascular, and displays faint cyclical growth marks. These marks are broadly spaced in the core of the ridges and tightly in their lateral layers (Fig. 11B). Short Sharpey's fibers occur as dense bundles in the core of the ridges. The *Acipenser* opercular shows no sign of inner or outer remodeling by the typical process of resorption followed by reconstruction. However, broad erosion bays perforate the superficial cortex in all parts, and result either in the differentiation of ridges through the erosion of vertical bone blades, or to a general reshaping of the ridges (Fig. 11A,E). This resorption process occurs inside the ornamented cortex, not on its surface.

Histological observations suggest that the creation and growth of ornamental reliefs on the *Acipenser* opercular mainly depends on the development of the ridges. The latter result from local acceleration of bone accretion, as evidenced by both the basic histological

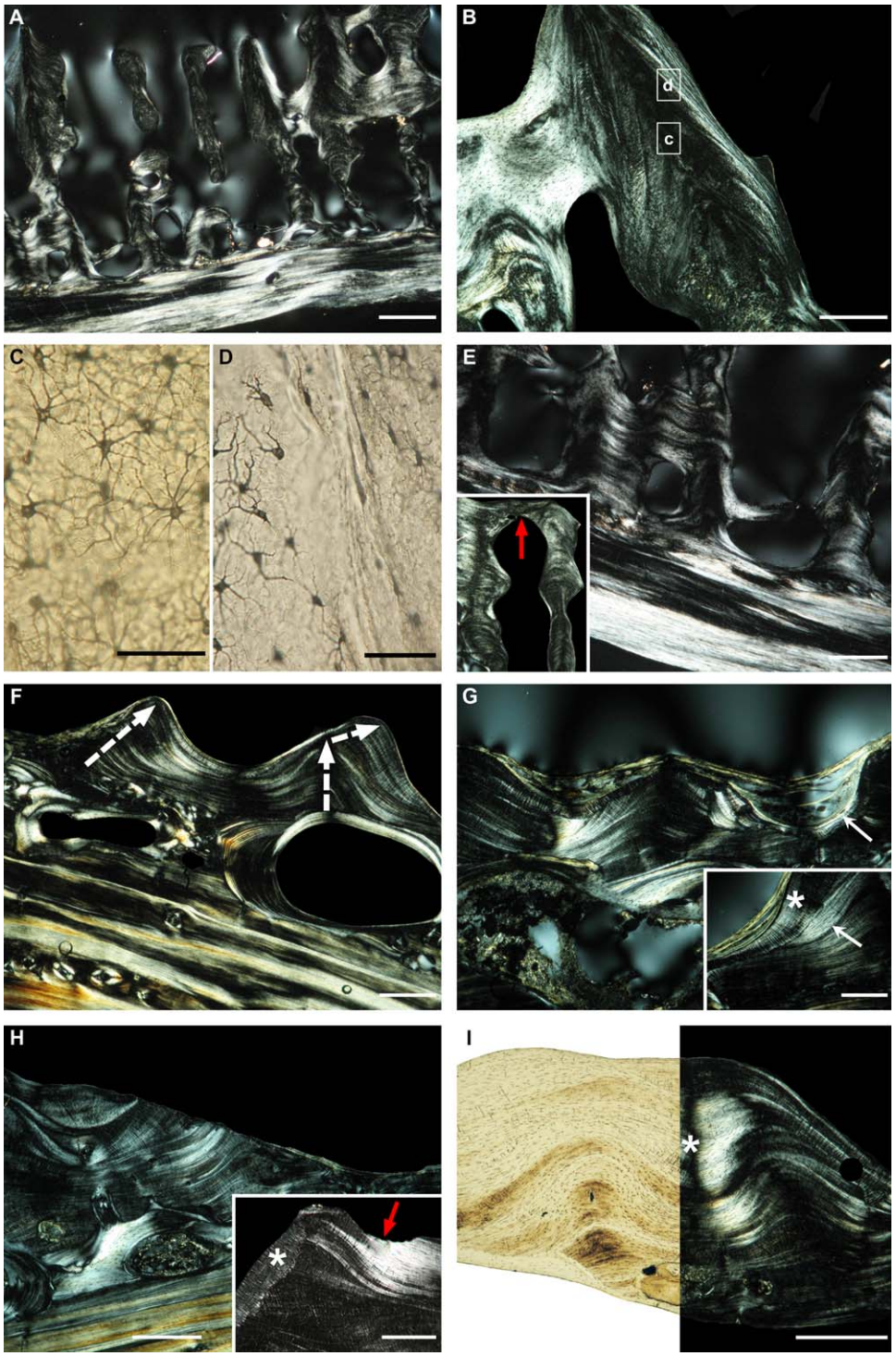

Fig. 11. General histology of ornamented bones in the extant actinopterygians *Acipenser sturio* (**A–E**) and *Arapaima gigas* (**F–I**). **A**: General microstructural organization of an *Acipenser* opercular (polarized light). **B**: Histological structure of a ridge. The core of the ridge is poorly birefringent, while its sides display bright birefringence. The closer fields shown in figures C and D are indicated (polarized light). **C**: Multipolar osteocyte lacunae with long canaliculi in the core of a ridge. **D**: Spindle-like osteocyte lacunae devoid of canaliculi in the lateral sides of a ridge. **E**: Inner resorption in the superficial cortex (the basal one is not resorbed). Insert: reshaping of a ridge by inner resorption (arrow) (polarized light). **F**: General structure of an *Arapaima* opercular (polarized light). Both cortices are birefringent. Ridges are drifting during growth (dashed arrows). **G**: Superficial process of resorption and reconstruction in the ornamented layer. Reversion lines (arrows) and secondary reconstruction deposits (asterisk) are obvious. **H**: Active resorption (by the time the animal died) in an *Arapaima* opercular (main frame). The insert shows Howship's lacunae created by active resorption (red arrow) on top of a ridge, along with reconstruction deposit (asterisk) on the side of the same ridge (polarized light). **I**: Filling of a pit (asterisk) in an *Arapaima* opercular (right frame in polarized light). Scale bars: A = 1 mm; B, E main frame, F, H main frame, I = 500 μm; G main frame and insert, H insert = 250 μm; C, D = 50 μm.

traits of the tissue in the core of the ridges (as compared to the basal cortex and ridge sides), and the spacing of growth marks. In addition to this basal process, a strong activity of inner resorption, not followed by reconstruction, modifies the whole geometry of the ridge network, and makes the pits deeper by eroding their floors from inside.

Osteoglossiformes (*Arapaima gigas*). The opercular of *Arapaima gigas* has a diploe architecture, and a simple histological structure: it comprises two (basal and superficial) cortices made of the same kind of osseous tissue. The latter is a brightly birefringent avascular parallel-fibered bone displaying cyclic growth marks in the form of faint annuli (Fig. 11F). The annuli and the bone strata forming the floor of the pits have histological traits close to those of the lamellar bone tissue. Conversely, the ridge core comprises a less birefringent tissue (Fig. 11F,G). Both cortices house abundant, short Sharpey's fibers. Active remodeling occurs in the central part of the opercular, transforming the deep strata of the cortices into a loose spongiosa (Fig. 11F). The superficial, ornamented cortex displays evidence of extensive remodeling, in the form of reversion lines separating discordant bone deposits (Fig. 11G), along with Howship's lacunae (Fig. 11H). The whole surface of the ornamented cortex is involved and (as described above in turtles) reconstructive bone deposits extend to both the floor of the pits, where they constitute secondary deposits, and the top of the ridges, where they can either represent secondary or primary bone deposits. Several subsequent resorption/reconstruction cycles occur in some areas (Fig. 11H).

According to these histological observations, differentiation and growth of ornamental reliefs in *Arapaima* opercular result from a double mechanism: 1) the commonly-observed discrepancy in accretion rate between pit bottom (slow accretion) and ridge top (faster accretion); 2) an extensive, patchy remodeling of ornamented surfaces by cycles of resorption and subsequent reconstruction. Additionally, the common processes of ridge drift (Fig. 11F) and pit filling (Fig. 11I) observed in most taxa occur also in *Arapaima*.

Siluriformes (*Phractocephalus hemioliopterus* and *Sciades proops*)

The *Phractocephalus* opercular features a typical diploe (Fig. 12A) of relatively low compactness (78.8%). The general histological structure of this bone closely resembles that observed in most temnospondyl bones: the whole basal cortex, the parts of the superficial cortex forming the floor of the pits, and the lateral sides of the ridges are made of birefringent parallel-fibered tissue (Fig. 12A,C,E). This tissue is basically avascular and non-remodeled; however, limited Haversian remodeling occurs in the floor of some pits (Fig. 12C). The core of the ridges is made of a poorly birefringent tissue structurally halfway between the parallel-fibered and the woven-fibered types (Fig. 12C,D). Annuli, more broadly spaced in the axial region of the ridges than in the floor of the pits, occur in both the superficial and basal cortices (Fig. 12D,E). Vascular canals (primary osteons and simple canals) mainly occupy the base of the ridges, and can be ramified. The central spongiosa of the opercular, made of a coarse woven-fibered tissue that tends to stretch into the core of the ridges, is intensely remodeled. With the exception for some secondary osteons located in the floor of some pits, the ornamented layer displays no trace of remodeling, and lacks deep or superficial resorption traces such as reversion lines or Howship's lacunae. The superficial cortex is in continuity with subjacent bone layers, and gradually merges with them (Fig. 12C,D).

The histological characteristics of the opercular (primary bone deposits, spacing of growth marks) suggest that bone accretion rate is more elevated on top of the ridges than on the floor of the pits. This sole difference suffices to explain the creation and growth of ornamental reliefs. During growth, the ridges are subject to the same processes of lateral drift (Fig. 12A) or width reduction (Fig. 12D) as those observed in the temnospondyls. Moreover, pits can be filled up and replaced in situ by ridges, a process resulting from a steep increase in local accretion rate, as suggested by vascular proliferation at those spots (Fig. 12E).

The opercular of the second siluriform species, *Sciades proops*, has a simple structure with two cortices (basal and superficial ornamented) framing a central cancellous region (Fig. 12F). The basal cortex is made of well-characterized lamellar bone tissue, whereas the superficial one is made of both poorly birefringent parallel-fibered bone in the core of the ridges, and brightly birefringent lamellar tissue in the floor of the pits (Fig. 12F,G). Cyclical growth marks in the form of lines of arrested growth are conspicuous in the core of the ridges (Fig. 12G). Their spacing clearly reveals that accretion rate was maximal on the top of the ridges and minimal on their sides. The central spongiosa results from a complex resorption process that creates broad erosion bays in the deep strata of the ornamented cortex, especially in the floor of the pits (Fig. 12F,H). Two additional differences distinguish the basal and the superficial cortices: 1) the basal cortex lacks Sharpey's fibers whereas the superficial one is entirely colonized by very dense bundles of long fibers with a fan-like arrangement, especially in ridges (Fig. 12G insert); 2) the basal cortex shows no sign of remodeling; conversely, the ornamented cortex is extensively and intensively remodeled. Bone remodeling, characteristically evidenced by resorption lines and discordant bone deposits, takes place

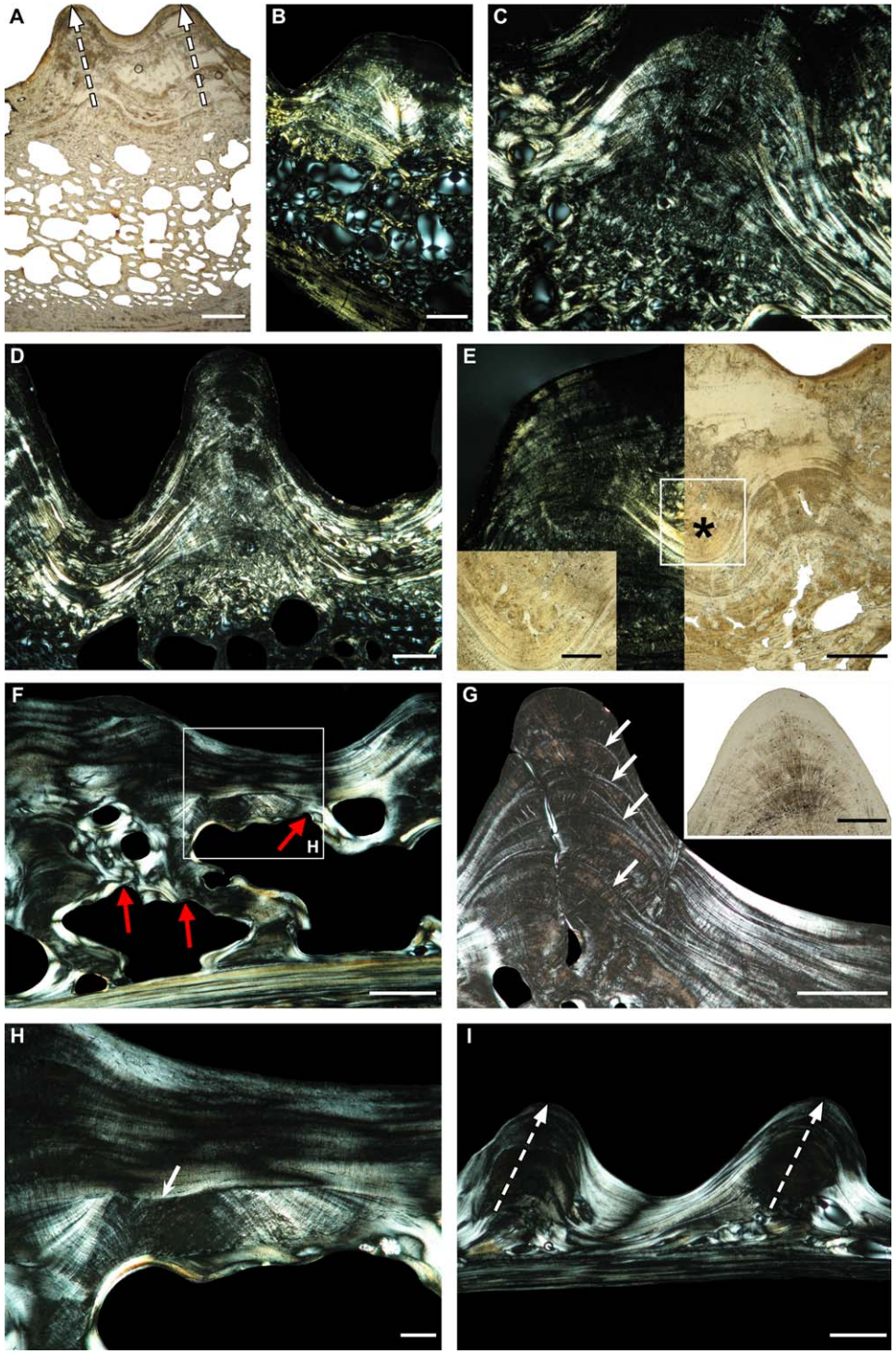

Fig. 12. General histology of ornamented bones in the extant teleosts *Phractocephalus hemioliopterus* (**A–E**) and *Sciades proops* (**F–I**). **A**: general diploe structure of a *Phractocephalus* opercular. Dashed arrows point to the sub-parallel drift of ridges during growth. **B**: General structure of the same bone in polarized light. Both the basal and superficial cortices are birefringent. **C**: Basic bone histology in ridge and pit (transmitted polarized light). Birefringence is poor in the core of the ridge, and there is no reversion line or discordant bone deposits between the superficial and the deeper layers. **D**: Decrease in ridge width during growth (polarized light). **E**: Pit filling during growth. Local vascular density is increased (insert showing enlargement of the framed field), which suggests that pit filling (asterisk) is due to acceleration in accretion (right half and insert: ordinary transmitted light; left frame: polarized light). **F**: General inner architecture of a *Sciades* opercular. The deep strata of the superficial cortex are submitted to intense and extensive remodeling initiated by resorption (red arrows) (polarized light). **G**: Bone histology in a ridge of the same bone (main frame: polarized light; insert: natural transmitted light). The core of the ridges is made of a poorly birefringent tissue displaying cyclical lines of arrested growth (arrows). The view in the insert shows the abundance of Sharpey's fibers in this bone. **H**: Reversion line (arrow) and discordant bone deposits in the superficial layer (polarized light). **I**: Sub-parallel lateral drift of two ridges (dashed arrows) (polarized light). Scale bars: A, B = 1 mm; C-F, I = 500 μm; E insert, G main frame = 250 μm; G insert = 200 μm; H = 100 μm.

on the surface of the ornamental reliefs as well as in the depth of the cortex, especially in the floor of the pits (Fig. 12H). This process spreads over the whole surface of the ornamented layer.

Histological observations suggest that the differentiation and growth of bone ornamentation on the opercular of *Sciades proops* results from the combination of three processes: 1) faster growth on top of the ridges; 2) resorption of pit bottom provoking an increase in pit depth; 3) extensive remodeling of the ornamented surface through resorption and reconstruction. Additionally, the common processes of ridge drift (Fig. 12I), and pit filling occur also in *Sciades* opercular.

Dipnomorpha

Porolepiformes (*Holoptychius*). The scale of *Holoptychius* is not a diploe but a compact (95–97%) solid bone organized in two very distinct layers: a totally avascular basal stratum some 1.8 mm in mean thickness and a superficial layer of variable thickness (0.5–1 mm) densely vascularized by a reticular-like network of wide (diameter *ca*. 50 μm) vascular canals (Fig. 13A). Scale ornamentation is displayed by this second layer. The basal layer is made of typical orthogonal (though slightly irregular) osseous plywood displaying 10–20 bone strata (depending on the area) alternatively light and dark in transmitted polarized light. The dark strata are 100–120 μm in thickness and display big clusters (some 10–12 μm in diameter) of fibers sectioned transversely. The light strata (80–90 μm in thickness) are made of a homogeneous, strongly birefringent tissue (Fig. 13B). Osteocyte lacunae are visible neither in the dark nor in the light strata. Both kinds of strata are actually made of the same type of osseous tissue, pure parallel-fibered bone; the different aspects that they show in polarized light are due to their orthogonal orientation. This description is in agreement with that of the "non-stabilized orthogonal" plywood in the basal layer of elasmoid scales described by Meunier and Castanet (1982; see also Meunier, 1984; Francillon-Vieillot et al., 1990).

The transition between the basal plywood layer and the superficial, densely vascularized layer is very steep and clear-cut; however these layers are separated by no discontinuity such as a reversion line or any trace of a resorption process that could have occurred before the deposit of the superficial layer (Fig. 13C). The ornamented layer mainly consists of a complex assemblage of unevenly oriented big primary osteons (Fig. 13C–E). Traces of primary periosteal tissue between the osteons are extremely sparse and of uncertain interpretation. Bone structure in some regions of the sections suggests that this tissue could be of the same kind as that composing the dark strata of the plywood layer, that is, parallel-fibered bone with fiber bundles oriented perpendicular to the sectional plane. Bone ornamentation does not correspond to any precise histological detail in the structure of the superficial layer, with exception for a slight difference in the density of the vascular canals in the ridges, where canal density is high, and the bottom of the pits, where it is lower (Fig. 13A). This difference suggests that ornamental reliefs result from a slight difference in accretion rate between the top of the ridges and the bottom of the pits. Apparently, no other osteogenic process was involved in the differentiation and growth of *Holoptychius* ornamentation; in particular, the scale displays no evidence of superficial remodeling, ridge drift or pit filling. Among the various taxa examined hitherto in this study, only the ornamented cortex of *Benthosuchus* skull bone displays similar histological features as those observed in the *Holoptychius* scale.

Synthesis of Results: Basic Osteogenic Mechanisms Controlling Ornamentation Growth

The entire set of histological observations presented above allows the distinction of six main mechanisms involved in the differentiation and growth of bone ornamentation. These mechanisms are briefly described below, and sketched in Figure 14, with indication of the basic osteogenic processes (given here in the sequence of their occurrence) from which they result, as listed in Table 2.

1. Neither resorption nor remodeling are involved (Fig. 14A)
   i. Simple difference in accretion rate between ridges (high rate) and pit floor (low rate). This basic process of differential growth (Fig. 14A1) does not necessarily imply that bone accretion is accelerated on top of the ridges, as compared to the basal cortex of the bones, but that growth in pits is slower. Differential growth is compatible with various primary bone tissue types, and often associated with the various other processes listed below. When it is the sole active process, then pit enlargement during growth is limited, depending mainly on divergent ridge drift, or reduction in ridge width. Pit filling is frequent.
   ii. Acceleration of bone accretion on the ridges. In this process (Fig. 14A2), growth is faster, in absolute terms, on top of the ridges than elsewhere on a bone. It is revealed by the histological structure of osseous strata in the core of the ridges, as compared to those occurring in both the floor of the pits and the basal cortex of the bone. Pit enlargement is then controlled by the same mechanisms as those mentioned for the preceding case. This process is very widespread, and was observed in several taxa, but with great local variations.

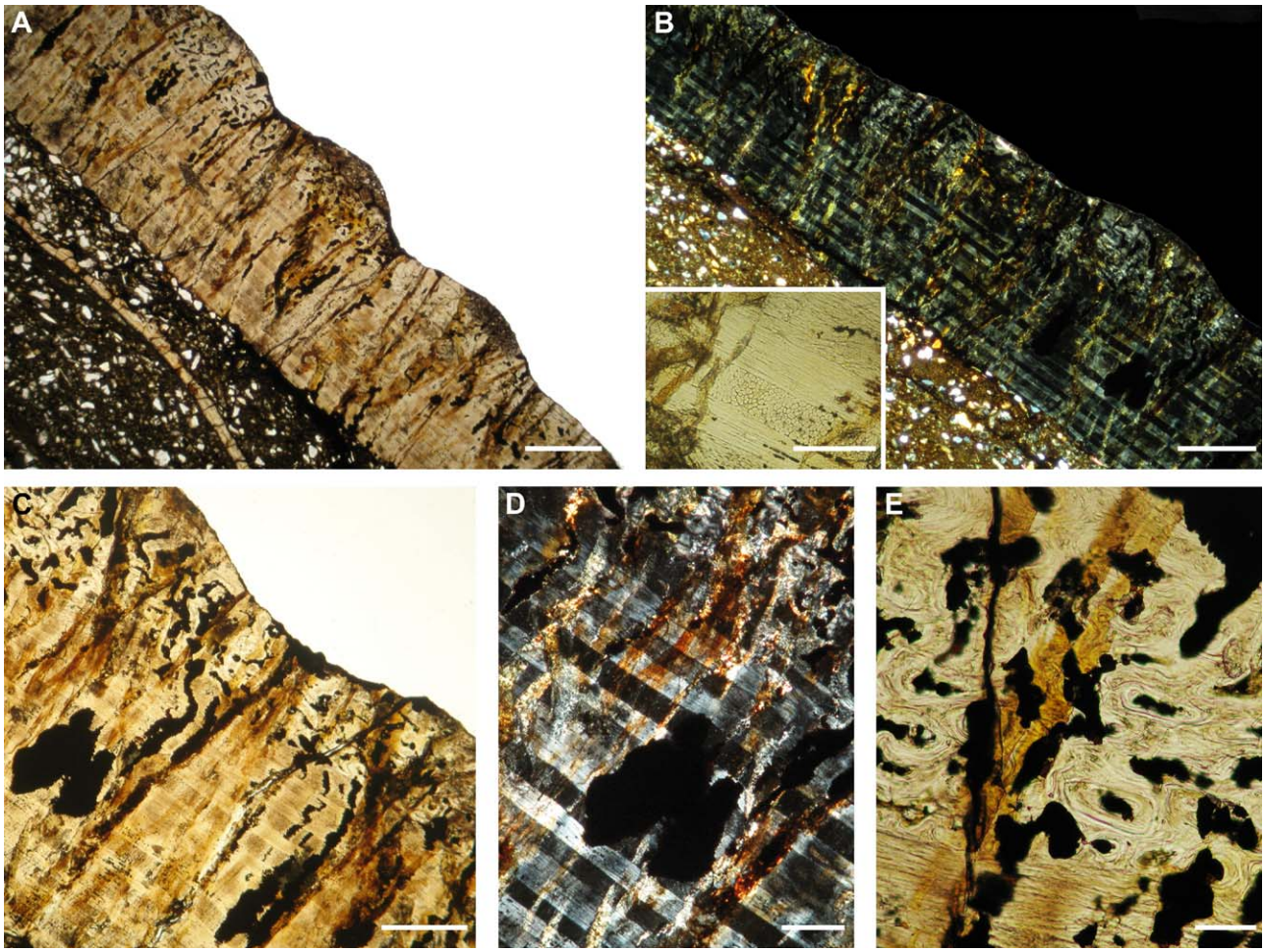

Fig. 13. Histology of the scale of the Late Devonian sarcopterygian *Holoptychius*. **A**: General structure of the scale. Two layers are visible: basal avascular plywood; densely vascularized superficial (ornamented) layer. **B**: Histological structure of the scale in polarized light (main frame), with detail of the plywood structure in natural light (insert). **C**: Detail of the transition zone between the basal plywood and the superficial vascularized layer. There is no discontinuity (e.g., reversion line) between this layer and the subjacent plywood. **D**: Closer view at the transition zone (polarized light). Again, no discontinuity separates the plywood from the superficial layer. **E**: Complex, histological organization of the superficial ornamented layer. Scale bars: A, B main frame = 1 mm; C = 500 μm; D = 250 μm; B insert = 200 μm; E = 100 μm.

2. Resorption or remodeling are involved (Fig. 14B–F)
   i. Extensive, continuous resorption of bone surface prior to the development of a secondary layer that bears ornamentation (Fig. 14B,C). The resorption process may result either in entire flattening of the bone surface (so called "flat integral resorption" hereafter; Fig. 14B) before the accretion of the ornamented layer (as exemplified by *Amyda cartilaginea*), or in the formation of initial reliefs that shall be further amplified (called below "curvy integral resorption"; Fig. 14C) by subsequent bone deposits. In both cases, the secondary, ornamented layer is of the parallel-fibered type and the creation (or amplification) of the ornamental reliefs is due to one of the two processes defined above, i.e. differential growth with (Fig. 14B2,C2) or without (Fig. 14B1,C1) acceleration on top of the ridges.
   ii. Creation of pits by isolated resorption spots (patchy resorption) on bone surface, with subsequent local (patchy) reconstruction (Fig. 14D). In the present sample, this typical remodeling process is well-represented by the actinopterygian *Arapaima*, the lissamphibians *Ceratophrys* and *Thaumastosaurus*, and the turtle *Araripemys*. It allows permanent and flexible modification (reshaping) of bone ornamentation at both local (e.g., one single pit or ridge) and general (the whole set of pits on a bone surface) scales. This process thus makes a fine dimensional accommodation of bone ornamentation to global skeletal growth possible (in addition to contributing to calcium and phosphorus recycling; cf. Dacke, 1979). Bone accretion on the ridges can be accelerated (Fig. 14D2) or not (Fig. 14D1).

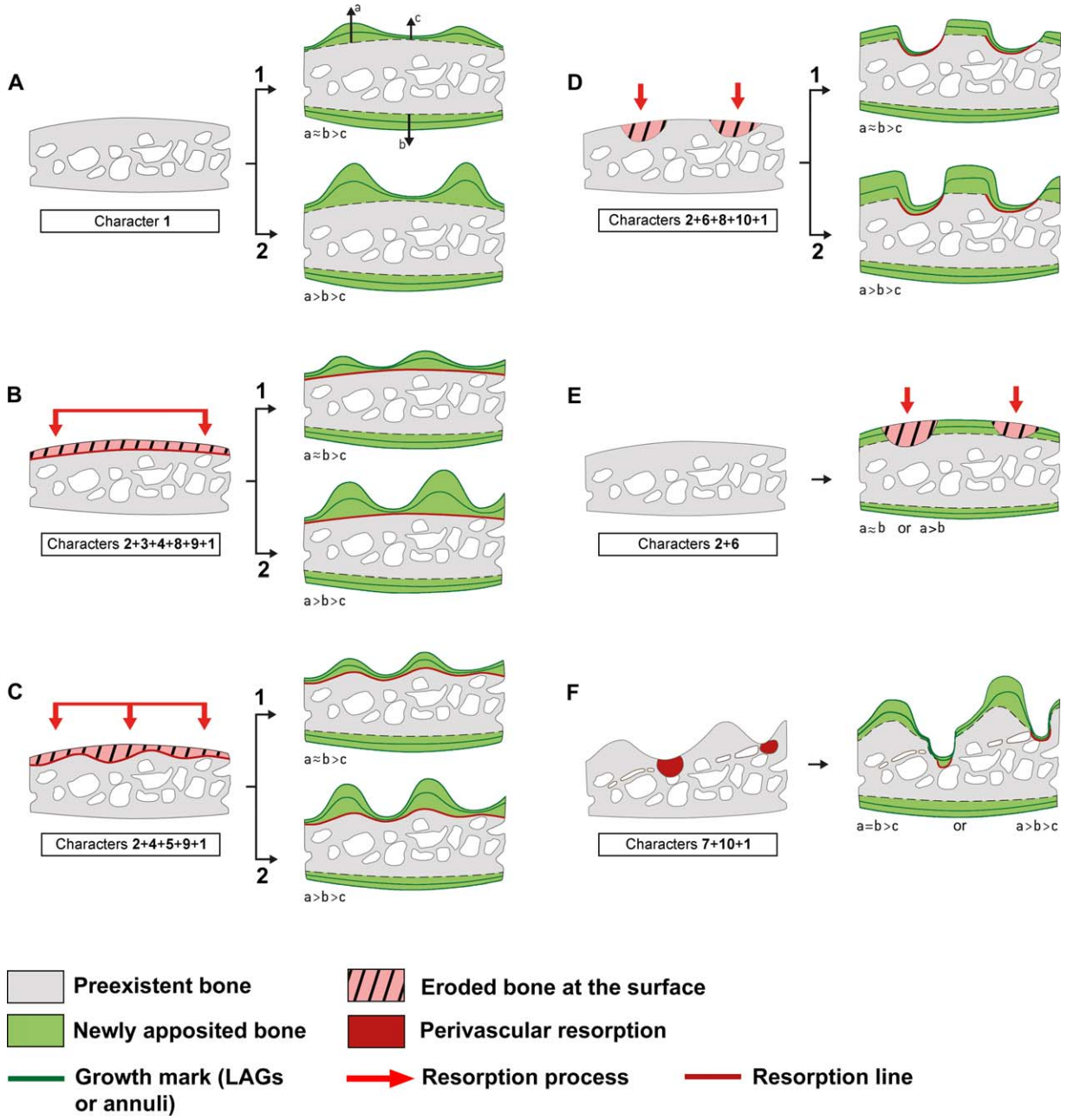

Fig. 14. Schematic representations of the six main mechanisms controlling the differentiation and growth of bone ornamentation, as observed in the sample. For each of these mechanisms, the numbers given in the rectangles refer to the basic osteogenic processes, indicated in Table 2 as "characters", which are sequentially involved in ornamentation morphogenesis. **A1**: Ornamentation is created by simple differential growth. Apposition rate during two growth cycles (green surfaces and green lines) on the ridges (a) is equal to that on the basal cortex (b), and higher to that on pit floor (c). **A2**: Ridge elevation through acceleration of bone apposition ($a > b > c$). **B**: Extensive resorption creating a flat surface prior to the formation of ornamental reliefs. The resorption process sets in place a resorption line (red line). The subsequent bone deposit on the superficial cortex may create ridges through simple differential growth (**B1**) or acceleration (**B2**). **C**: Extensive resorption creates a first outline of ornamental reliefs that is further enhanced in subsequent growth by simple differential growth (**C1**) or acceleration on the ridge (**C2**). **D**: Superficial remodeling of the ornamented cortex. Patchy, discontinuous resorption creates initial pits. Subsequent bone deposits without (**D1**) or with (**D2**) acceleration on ridges create ridges and reconstruct the eroded part of pit floors. In this case, resorption lines and secondary deposits are limited to pit floor. **E**: Pits are created by simple resorption of the superficial cortex, with no subsequent reconstruction. This process is likely to take place at the end of the growth period. F: Intra-cortical erosion of pit floor, with limited, subsequent reconstruction. This process is mainly perivascular. Various configurations may occur for the rate of bone deposition on top of the ridges.

TABLE 2. Character states (numbers in brackets) representing the basic osteogenic processes responsible for the differentiation of the pit and ridge type of bone ornamentation in Vertebrates

	Taxon	Differential Growth (1)	Resorption (2)	Integral Resorption (3)	Flat integral Resorption (4)	Curvy integral Resorption (5)	Patchy superf. Resorption (6)	Inner Resorption (7)	Reconstruction (8)	Continuous Reconstruction (9)	Patchy Reconstruction (10)	Source
PLACODERMI												
Arthrodira	*Incisoscutum* sp.	1	0	0	0	0	0	0	0	0	0	1
	Bothriolepis canadensis	1	0	0	0	0	0	0	0	0	0	2
ACTINOPTERYGII												
Acipenseriformes	*Acipenser sturio*	1	1	0	0	0	0	1	0	0	0	PS
Neopterygii	*Phractocephalus hemioliopterus*	1	0	0	0	0	0	0	0	0	0	PS
	Sciades proops	1	1	1	0	1	0	1	1	1	0	PS
	Arapaima gigas	1	1	0	0	0	1	0	1	0	1	PS
SARCOPTERYGII	*Holoptychius* sp.	1	0	0	0	0	0	0	0	0	0	PS
Stegocephali												
Temnospondyli	*Eryops megacephalus*	1	0	0	0	0	0	0	0	0	0	PS
	Kupferzellia sp.	1	0	0	0	0	0	0	0	0	0	PS
	Mastodonsaurus sp.	1	0	0	0	0	0	0	0	0	0	PS
	Parotosuchus sp.	1	0	0	0	0	0	0	0	0	0	PS
	Peltobatrachus sp.	1	0	0	0	0	0	0	0	0	0	PS
	Platyoposaurus sp.	1	0	0	0	0	0	0	0	0	0	0
	Plagiosternum sp.	1	0	0	0	0	0	0	0	0	0	PS
	Trimerorachis insignis	1	0	0	0	0	0	0	0	0	0	PS
	Benthosuchus sushkini	1	0	0	0	0	0	0	0	0	0	PS
	Metoposaurus diagnosticus	1	0	0	0	0	0	0	0	0	0	3
	Dutuitosaurus ouazzoui	1	0	0	0	0	0	0	0	0	0	PS
	Indet. sp.	1	0	0	0	0	0	0	0	0	0	PS
	Stanocephalosaurus sp.	1	0	0	0	0	0	0	0	0	0	PS
Embolomeri	*Archeria* sp.	1	0	0	0	0	0	0	0	0	0	PS
Chroniosuchia	*Chroniosaurus dongusensis*	?	1	0	0	0	1	0	1	0	1	4
	Uralerpeton tverdochlebovae	1	0	0	0	0	0	0	0	0	0	5
	Bystrowiana cf. permiria	1	0	0	0	0	0	0	0	0	0	PS
Nectridea	*Diplocaulus* sp.	1	0	0	0	0	0	0	0	0	0	PS
Lissamphibia	*Ceratophrys* sp.	1	1	0	0	0	1	0	1	0	1	PS
	Indet. cf. *Thaumastosaurus*	1	1	0	0	0	1	0	1	0	1	PS
	Latonia gigantea	1	1	0	0	0	1	1	1	0	1	PS
Amniota	*Captorhinus aguti*	1	0	0	0	0	0	0	0	0	0	PS
	Condorchelys antiqua	1	1	0	0	0	1	0	1	0	1	5
	Aspideretoides sp.	1	1	1	1	0	0	0	1	1	0	PS, 6
	Glyptops plicatulus	1	0	0	0	0	0	0	0	0	0	7
	Stupendemys geographicus	?	1	0	0	0	1	0	1	0	1	8
	Amyda cartilaginea	1	1	1	1	0	0	0	1	1	0	PS
	Trionyx triunguis	1	1	1	1	0	0	0	1	1	0	PS
	Trionyx triunguis foss.	1	1	1	1	0	0	0	1	1	0	PS
	Cyclanorbis senegalensis	1	1	1	0	1	0	0	1	1	0	PS
	Pseudemys rubriventris	1	1	0	0	0	1	0	0	0	0	PS

Table 2. (continued).

Taxon	Differential Growth (1)	Resorption (2)	Integral Resorption (3)	Flat integral Resorption (4)	Curvy integral Resorption (5)	Patchy superf. Resorption (6)	Inner Resorption (7)	Reconstruction (8)	Continuous Reconstruction (9)	Patchy Reconstruction (10)	Source
Araripemys barretoi	1	1	0	0	0	1	0	0	0	1	PS
Necrosaurus cayluxensis	0	1	0	0	0	1	0	0	0	0	PS
Crocodyliformes (all taxa)	1	1	0	0	0	1	0	1	0	1	9
Phytosauria	1	1	0	0	0	1	0	1	0	1	9, 10
Doswelliidae	1	1	0	0	0	1	0	1	0	1	11
Aetosauria	1	1	0	0	0	1	0	1	0	1	12, 10
Revueltosaurus callenderi	1	1	0	0	0	1	0	1	0	1	10
Jaxtasuchus salomoni	1	1	0	0	0	1	0	1	0	1	10
Lupeosaurus kayi	1	0	0	0	0	0	0	0	0	0	PS

Score 0: character absent; score 1: character present. The basic information for building this table originates from the present study (PS), or from published studies referenced by the following numbers: 1-Giles et al. (2013); 2-Downs and Donoghue (2009); 3-Witzmann (2009); 4-Buchwitz et al. (2012); 5-Cerda et al. (2015b); 6-Scheyer et al. (2012); 7-Scheyer and Anquetin (2008); 8-Scheyer and Sánchez-Villagra (2007); 9-Buffrénil et al. (2015); 10-Scheyer et al. (2014); 11-Cerda et al. (2015a); 12-Cerda and Desojo (2010).

iii. Creation or deepening of pits by isolated resorption spots on bone surface, with no subsequent reconstruction (Fig. 14E). This simple situation, mainly observed in the necrosaur specimens (and, to a lesser extent, the turtle *Pseudemys*), offers only two possibilities for pit growth during ontogeny: i) increase in diameter through additional resorption on pit periphery; ii) increase in depth through either resorption of pit floor or elevation of ridges. In the necrosaur osteoderms, simple pit excavation was the only mechanism that created ornamentation in flat osteoderms but, in keeled ones, it contributed to the accentuation of pre-existing bone reliefs. It seems likely (though more data are needed) that simple excavation of pits occurs by the end of somatic development in taxa that have limited growth, as exemplified here by the squamate taxon Necrosauridae. Theoretically, acceleration of bone accretion on top of the ridges is possible.

iv. Deep intraosseous resorption of pit floor (Fig. 14F). This process complements other basic morphogenetic mechanism such as differential growth. It involves a resorption activity, often linked to the course of vascular canals, occurring inside the bones, not on their surface. It allows deepening of the pits through the inner erosion and final opening of their floor. Partial reconstruction locally follows the resorption phase. This process, as all the others described above, can be associated or not with accelerated ridge growth. Morphologically, it results in deep, well-like pits, as exemplified by the chondrostean *Acipenser* or the anuran *Latonia*.

In order to have a synthetic view of the taxonomic distribution of these various morphogenetic mechanisms, considered through the basic osteogenic process from which they result, all the histological data about the differentiation and growth of the pit and ridge type of ornamentation, be they derived from the present study or from articles previously published by other authors, were collected and organized into Table 2 that was used to conduct the ML optimization study presented below. Of course, among the data obtained from literature, only those relative to the pit and ridge ornamentation type, and based on clear, unquestionable descriptions accompanied by sharp, explicit illustrations were retained.

Evolutionary Analyses

Evolutionary models can be used, to some extent, to test hypotheses. Our hypothesis is that resorption is selectively advantageous in the development of dermal ornamentation; therefore, forward rates should be higher than backward rates for characters reflecting this phenomenon. Assessing support

for evolutionary models is also a prerequisite to tracing character history, so results about models are presented before optimizations.

The ML analyses of the presence of resorption (character 2 in Table 2) on both topologies (Fig. 15) indicate that the two-rate model is better-supported than the single-rate model, though the difference in support between both models is greater when turtles are placed outside diapsids than among them (Table 3). In both cases, the forward rate is about 3–4 times greater than the backward rate. The occurrence of resorption probably displays the most reliable rates because it is the most variable in our sample; hence, there are more data to estimate the model parameters. This reflects the complexity of the evolutionary pattern of the character (Fig. 15), which appears to display four gains and one loss in stegocephalians, and a pattern more difficult to interpret in actinopterygians (but involving at least two events, possibly including a loss).

Limited additional support for our hypothesis can be gathered from other characters. For instance, for characters 6 (patchy superficial resorption) and 8 (reconstruction), the forward rate is also higher than the backward rate in the two-rate model, though little weight can be attached to this because the one-rate model is better supported, in both cases (Table 3).

A few characters seem to show greater backward than forward rates, but these estimates are probably not reliable. For instance, integral resorption (character 3) has forward and backward rates of 6.21 E-4 and 3.34 E-3 respectively, but these rates cannot be well-constrained because the character appears to display only two gains and no losses (Fig. 16A), and for this character, support for the one-rate model is nearly as great as for the two-rate model (Table 3). An even more instructive case is flat integral resorption (character 4), for which support for the two-rate model is about four times greater than for the one-rate model. For this character, the forward rate (3.81 E-4) is much smaller than the backward rate (6.61 E-3), but this appears to be also unreliable because the model infers the gain two nodes deeper than the most parsimonious position. This situation is presubably due to the short branches linking these nodes, and this forces two losses in the cryptodire turtles *Cyclanorbis* and *Pseudemys* (Fig. 16B). Curvy integral resorption (character 5) also has a greater backward than forward rate according to the two-rate model, but support for that model is less than for the one-rate model (Table 3), and only two gains (and no losses) can be inferred (Fig. 16C). Inner resorption (character 7) similarly shows a greater backward than forward rate according to the two-rate model, but support for that model is only half that for the one-rate model (Table 3), and only three gains (and no losses) can be inferred (Fig. 16D). Continuous reconstruction (character 9) has backward rates about five times greater than forward rates, but support for one- and two-parameter models is about equal (Table 3), and history of the character could be explained by two gains and no losses (Fig. 16F). Finally, for patchy reconstruction (character 10), the backward rate is greater than the forward rate, but the one-rate model has nearly three times more support than the two-rate model, so these estimates cannot be reliable (Table 3).

The ML optimizations (always illustrated and shown using the model with best support) show clearly that resorption (character 2) was absent in the development of ornamentation in the first gnathostomes (Fig. 15). Indeed, resorption is found only in a few clades; it appeared among actinopterygians (perhaps more often than parsimony suggests), among some chroniosuchians (in the Late Permian), among lissamphibians (it appears to prevail at least among anurans), and in most sauropsids. The details of this history are uncertain, as shown by the probabilities of the states at various nodes. The most uncertain part of this history is found among actinopterygians. At the base of the clade, both models under both topologies suggest that the probability that resorption was absent is around 0.73–0.75 (Fig. 15; Table 4). Higher up that clade, the probability that early teleosts lacked resorption decreases, a result consistent with the fact that two out of the three sampled teleosts show resorption (Fig. 15). By contrast, the condition at the base of sauropsids is relatively clear, with both models under both topologies yielding probabilities of resorption being absent in the process responsible for dermal sculpturing around 0.96–0.99 (Table 4). However, the uncertainty in the position of turtles results in substantial uncertainty about the condition in the first crown-reptiles. If turtles are diapsids (Fig. 15B), that ancestor probably used resorption in the development of dermal ornamentation; if turtles are outside diapsids, that ancestor (which then coincides with the basalmost node in Sauropsida) probably lacked resorption, a result partly attributable to the fact that the early eureptile *Captorhinus aguti* lacked such resorption, and partly because of the much greater age of the ancestor, under that topology (Fig. 15A).

The evolution of patchy resorption (character 6) follows a similar pattern, but given that patchy resorption is a special case of the presence of resorption, it has a less inclusive taxonomic distribution. Thus, this character is present only in *Arapaima*, among the sampled actinopterygians, so the character was probably ($0.9 < P < 0.96$) absent at the base of Actinopterygii (Table 4) and of Teleostei. The character was similarly absent at the base of Sauropsida ($0.98 < P < 1.00$), as expected (Table 4). However, within turtles, it either appeared three

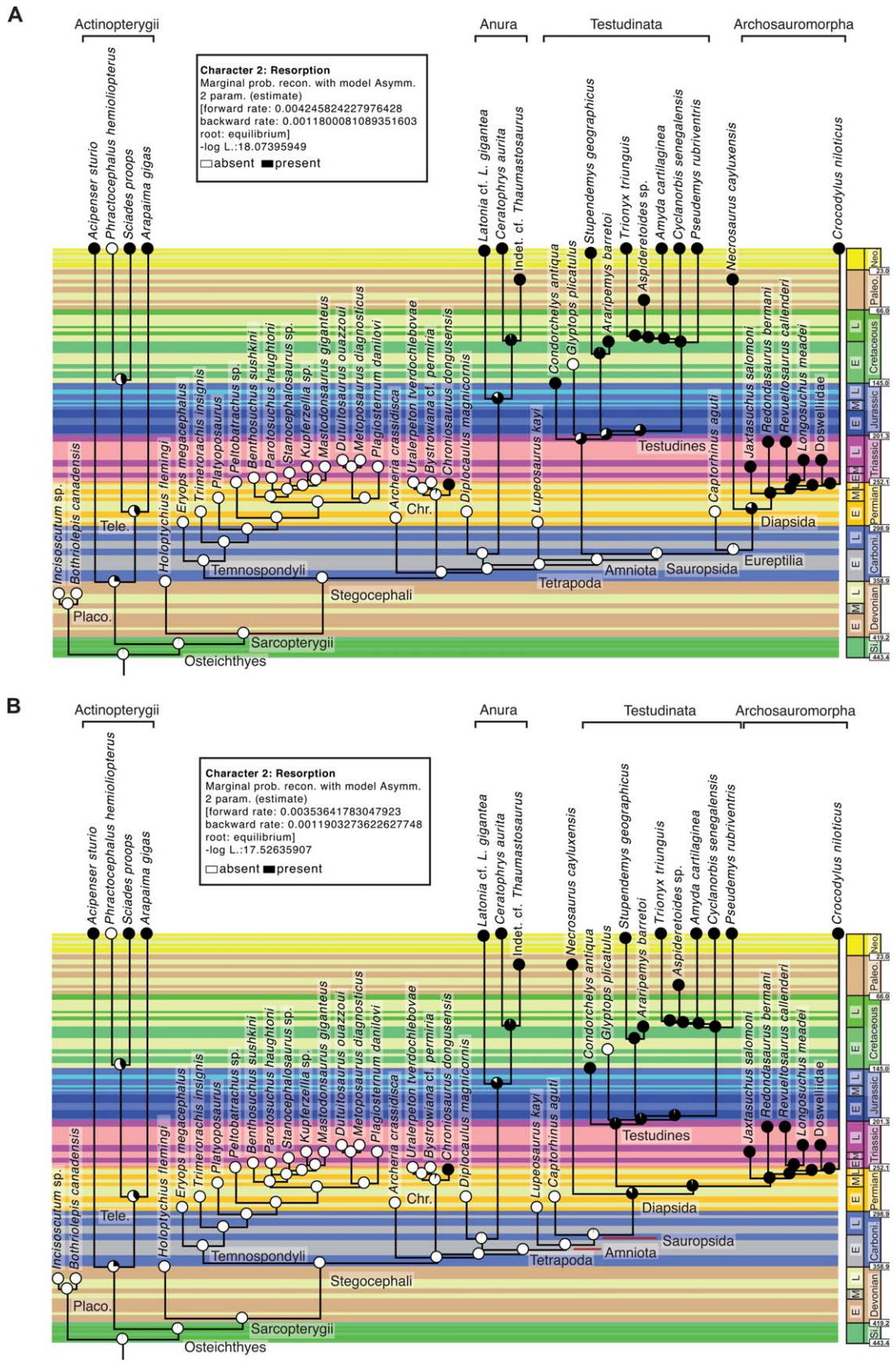

Fig. 15. Evolutionary pattern of the presence of resorption (character 2) in the developmental mechanism responsible for dermal ornamentation in gnathostomes. Maximum likelihood (ML) optimization performed in Mesquite 3.04. The relative extent of the black and white areas in the circles at the nodes indicate the probabilities of each state at that node (black: resorption; white: no resorption), according to the two-rate model of evolution, which is the best-supported model (Table 3). This graphic convention was introduced by Schluter et al. (1997). Two topologies are shown, one (A) with turtles outside Diapsida, and one (B) with turtles in diapsids, among archosauromorphs. Each horizontal colored band represents a geological stage from a recent time scale (Gradstein et al., 2012), though the names of these stages cannot appear on the figure for lack of space. Abbreviations for the names of the clades: Chr.: Chroniosuchia; Placo.: Placodermi; Tele.: Teleostei. Abbreviations for the geologic time scale: Carboni.: Carboniferous; E.: Early; L.: Late; M.: Middle; Neo: Neogene; Paleo.: Paleogene; Si.: Silurian.

TABLE 3. Assessment of evolutionary models of histological characters involved in the development of dermal ornamentation

Char.	Topology	Model	V	-log L.	Rate(s)	AIC	AICc	AICc weights
2, Res.	Test. (Lepi. Archo.)	Mk 1 rate	1	19.991	2.615 E-3	41.982	42.075	0.3056
		Mk 2 rates	2	18.074	F: 4.246 E-3; B: 1.180 E-3	40.148	40.434	0.6944
	Lepi. (Test. Archo.)	Mk 1 rate	1	18.872	2.157 E-3	39.745	39.838	0.4379
		Mk 2 rates	2	17.526	F: 3.536 E-3; B: 1.190 E-3	39.053	39.338	0.5621
3, Int. Res.	Lepi. (Test. Archo.)	Mk 1 rate	1	10.734	6.894 E-3	23.468	23.561	0.4883
		Mk 2 rates	2	9.591	F: 6.211 E-4; B: 3.338 E-3	23.182	23.467	0.5117
4, Flat Res.	Lepi. (Test. Archo.)	Mk 1 rate	1	9.915	3.244 E-4	21.831	21.924	0.2031
		Mk 2 rates	2	7.452	F: 3.813 E-4; B: 6.605 E-3	18.904	19.189	0.7969
5, Curv. Res.	Lepi. (Test. Archo.)	Mk 1 rate	1	8.425	5.075	18.839	18.942	0.5417
		Mk 2 rates	2	7.496	F: 7.006 E-4; B: 6.817 E-3	18.991	19.277	0.4583
6, Pat. Res.	Test. (Lepi. Archo.)	Mk 1 rate	1	20.885	2.559 E-3	43.770	43.863	0.6869
		Mk 2 rates	2	20.574	F: 2.631 E-3; B: 1.3086 E-3	45.148	45.434	0.3131
	Lepi. (Test. Archo.)	Mk 1 rate	1	20.593	2.414 E-3	43.185	43.278	0.7478
		Mk 2 rates	2	20.583	F: 2.482 E-3; B: 2.265 E-3	45.166	45.452	0.2522
7, Inner Res.	Lepi. (Test. Archo.)	Mk 1 rate	1	9.323	8.087 E-4	20.647	20.740	0.6460
		Mk 2 rates	2	8.829	F: 8.313 E-4; B: 3.021 E-3	21.657	21.943	0.3540
8, Rec.	Lepi. (Test. Archo.)	Mk 1 rate	1	22.299	3.656 E-3	46.599	46.692	0.7453
		Mk 2 rates	2	22.277	F: 3.846 E-3; B: 3.432 E-3	48.553	48.839	0.2547
9, Cont. Rec.	Lepi. (Test. Archo.)	Mk 1 rate	1	10.734	6.894 E-4	23.468	23.561	0.4883
		Mk 2 rates	2	9.591	F: 6.211 E-4; B: 3.338 E-3	23.181	23.467	0.5117
10, Pat. Rec.	Lepi. (Test. Archo.)	Mk 1 rate	1	19.587	2.166 E-3	41.173	41.266	0.7186
		Mk 2 rates	2	19.428	F: 1.936 E-3; B: 2.847 E-3	42.856	43.142	0.2814

In all cases, the sample size (n) is 45 taxa. Character 1 is invariable, so it is not shown. Only two characters (2 and 6) of particular relevance are analyzed on both trees.

Abbreviations: AIC: Akaike Information Criterion; AICc: Akaike Information Criterion corrected for small sample size; AICc weights: relative support for each model indicated by AICc; Archo.: Archosauria; B: backward transition rate; Char.: character; Con. Rec.: continuous reconstruction; Curv. Res.: curvy integral resorption; F: forward transition rate; Flat Res.: flat integral resorption; Inner Res.: inner resorption; Int. Res.: integral resorption; Lepi.: Lepidosauria; Mk 1 rate: Markov model with a single evolutionary rate; Mk 2 rates: Markov model with two evolutionary rates (a forward and a backward rate); Pat. Rec.: patchy reconstruction; Pat. Res.: patchy superficial resorption; Rec.: reconstruction; Res.: resorption; Test.: Testudinata; V: number of estimated parameters.

times convergently (and once in diapsids), if turtles are placed outside the Diapsida (Fig. 17A,B), or it appeared at the base of Sauropsida and was lost twice within turtles, if turtles are considered as diapsids (Fig. 17C,D). The evolutionary model (one or two parameters) affects the probabilities of ancestral states in that part of the tree, but much less than topology and branch lengths combined.

The evolution of other characters can be evoked briefly. Integral resorption (character 3) occurs only in the teleost *Sciades* and in most cryptodires (Fig. 16A), and flat integral resorption (character 4) occurs only in some cryptodires (Fig. 16B). Curvy integral resorption occurs only in one teleost and one cryptodire (Fig. 16C). Inner resorption (which starts within the bone, rather than at its surface) is also fairly uncommon; it occurs only in two teleosts and one anuran, which probably represent three independent acquisitions of this character (Fig. 16D). Reconstruction (character 8) occurs in most (but not all) taxa that have resorption (Fig. 16E). The exceptions concern the actinopterygian *Acipenser*, the squamate *Necrosaurus*, and the turtles *Araripemys* and *Pseudemys*. Thus, both character histories differ mostly by more losses in reconstruction (3.66 E-3, in the one-rate model, which has greatest AICc weight, and 3.43 E-3 in the two-rate model) than in resorption (1.18 E-3 in the two-rate model, which has greatest AICc weigth, and 2.16 E-3 in the one-rate model; both according to the topology with turtles in diapsids). Continuous reconstruction (character 9) is much rarer; it occurs in one teleost and most cryptodire turtles sampled here (Fig. 16F). Finally, patchy reconstruction (character 10) occurs in one teleost, one chroniosuchian, the sampled anurans, and most archosauromorphs (which include turtles, in the tree shown); this distribution suggests four appearances and a few reversals, which occur only within crown reptiles (Fig. 16G).

DISCUSSION

Comparative Overview

The new data presented above, as well as previously-published data show that bone ornamentation in most Paleozoic stegocephalians is produced by preferential apposition. Several descriptions of the histological structure of bones displaying the pit and ridge type of ornamentation have already been published, especially for Paleozoic stegocephalians (Bystrow, 1935; Witzmann, 2009; Witzmann and Soler-Gijón, 2010; Witzmann et al., 2010), turtles (Scheyer and Anquetin, 2008; Scheyer and Sánchez-Villagra, 2007; Scheyer et al., 2007), archosaurs (Cerda and Desojo, 2010; Scheyer et al., 2014; Buffrénil et al., 2015; Cerda et al., 2015a), and some other gnathostomes including placoderms (Downs

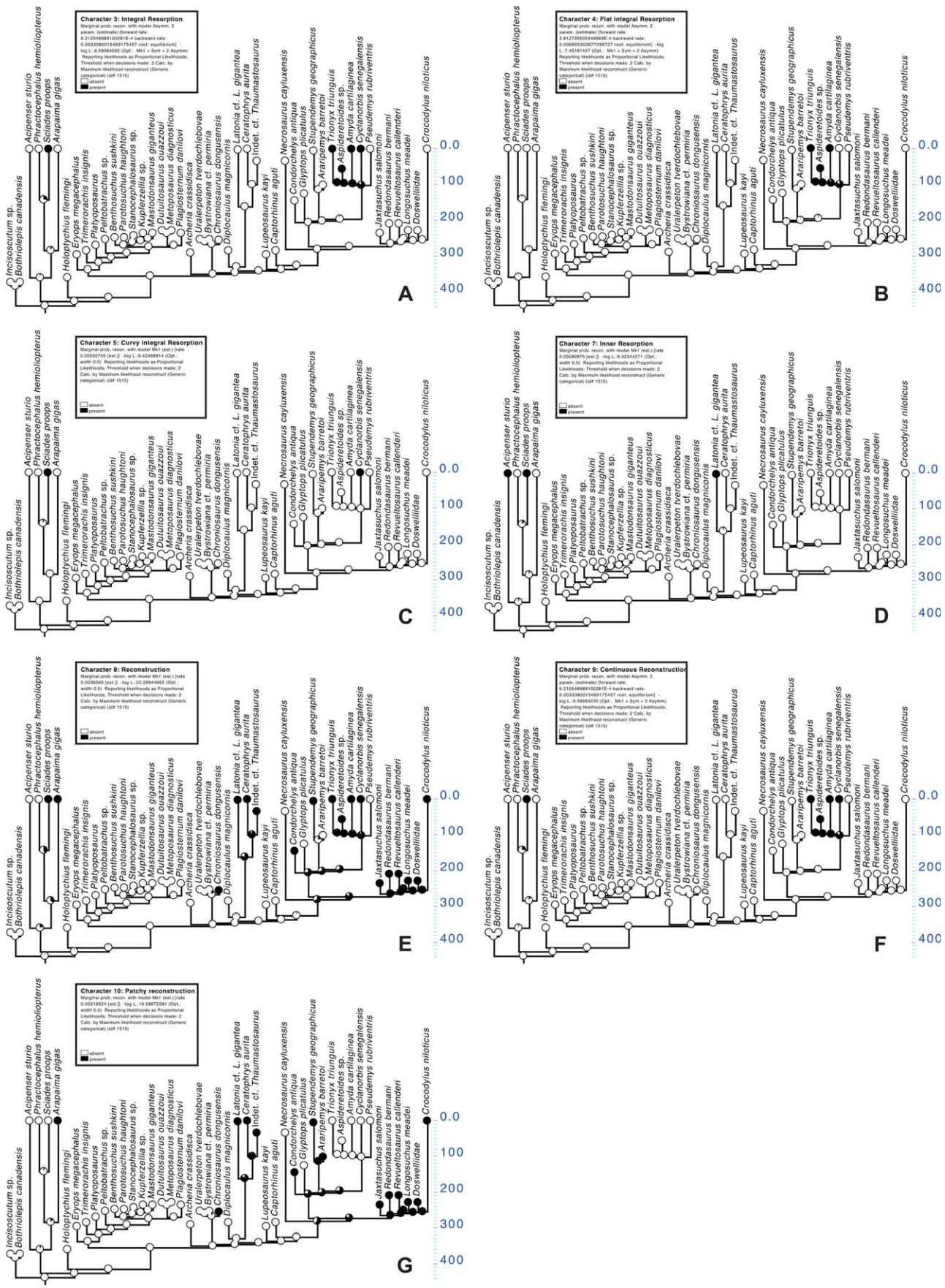

Fig. 16. Evolutionary pattern of the other histological characters linked with the development of dermal ornamentation. To save space, a single topology (with turtles in diapsids) is shown, and only the model with the greatest AICc weight is used to infer character history. For more information, see legend of Figure 15. **A**: Integral resorption (character 3), 2-rate model. **B**: Flat integral resorption (character 4), two-rate model. **C**: Curvy integral resorption (character 5), one-rate model. **D**: Inner resorption (character 7), one-rate model. **E**: Reconstruction (character 8), one-rate model. **F**: Continuous reconstruction (character 9), two-rate model. **G**: Patchy reconstruction (character 10), one-rate model.

TABLE 4. Ancestral states for two characters at selected nodes

Node	Character	Topology	P_0 Mk 1 rate	P_0 Mk 2 rates	P_0, model-averaged	P_1, model-averaged
Sauropsida	2. Resorption	Test. (Lepi. Archo.)	0.9598	0.9882	0.9795	0.0205
	2. Resorption	Lepi. (Test. Archo.)	0.9800	0.9883	0.9847	0.0153
	6. Patchy superficial resorption	Test. (Lepi. Archo.)	0.9809	0.9947	0.9852	0.0148
	6. Patchy superficial resorption	Lepi. (Test. Archo.)	0.9786	0.9800	0.9790	0.0210
Actinopterygii	2. Resorption	Test. (Lepi. Archo.)	0.7480	0.7389	0.7417	0.2583
	2. Resorption	Lepi. (Test. Archo.)	0.7391	0.7513	0.7460	0.2540
	6. Patchy superficial resorption	Test. (Lepi. Archo.)	0.9065	0.9530	0.9210	0.0790
	6. Patchy superficial resorption	Lepi. (Test. Archo.)	0.9157	0.9183	0.9164	0.0836

Abbreviations: Archo.: Archosauria; Lepi.: Lepidosauria; Mk 1 rate: Markov model with a single evolutionary rate; Mk 2 rates: Markov model with two rates (forward and backward); P_0: probability that state 0 was present, according to a given model; P_1: probability that state 1 was present, according to a given model; Test.: Testudinata.

and Donoghue, 2009; Giles et al., 2013). As a consequence, histological studies of dermal bones in most of the temnospondyl, lepospondyl and a few amniote taxa used in the present work are already available in the literature. A detailed comparison between our observations and those previously published would be of limited interest because the details of bone structure (e.g., nature, density and orientation of vascular canals, characteristics of cell lacunae, etc.) are prone to substantial variation between conspecific specimens, bones of a single skeleton, and even the parts of a section. Assessing the importance of this variability in all the taxa that we used is beyond the scope of this study, and would require a much broader sample to be performed. This is why the information that we consider most significant for our purpose are the gross osteogenic events unambiguously displayed by bone sections, that is, the occurrence or absence of superficial bone resorption (followed or not by reconstruction), as well as the nature of local bone tissues (woven-fibered, parallel-fibered, or true lamellar bone) and their vascular supply. The latter features are considered together, in the particular context of each section, as a set of clues revealing local trends in appositional rates, as exposed above (see "Basic clues for interpreting relative bone growth rates" in the Material and Methods section).

For Paleozoic stegocephalians, the histological descriptions presented here generally agree with published data regarding the most relevant question: the creation and growth of ornamental reliefs is basically due to preferential growth on top of the ridges, and excludes significant contribution of superficial resorption, as clearly settled by Witzmann and Soler-Gijón (2010; also see Bystrow, 1935, 1947 and Vickaryous and Hall, 2008). The only exception is relative to some Paleozoic stegocephalians (chroniosuchians) that have been considered either stem-tetrapods (Laurin, 2000; Vallin and Laurin, 2004), as our reference tree shows, or reptiliomorphs (Clack and Klembara, 2009; Schoch et al., 2010), and which are considered in more detail below.

This study further documents the mechanisms contributing to ornamentation growth in basal tetrapods by substantiating the concept of "preferential growth". The latter does not necessarily mean that absolute growth rate is increased on the ridges, as compared to the basal cortex, but that there is a local difference of speed (that difference can be pronounced or slight) between bone apposition on ridge top and on pit floor. Rather than "preferential" growth, the actual process involved is thus "differential" growth, although a real acceleration in local accretion may occasionally occur, especially when a pit is filled up and replaced *in situ* by a ridge.

Because Sharpey's fibers are generally much more abundant in ridges than in pit floors, they have been suspected to induce this differential growth process through traction on bone surface (Witzmann and Soler-Gijón, 2010). The results of the present study confirm that anchorage fibers are unevenly distributed within ornamented cortices; however, their role in the development of ornamental reliefs remains to be ascertained. For the present, this hypothesis indeed fails to explain why ornamentation appears only on the superficial (often dorsal) side of osteoderms, while both sides can be firmly bound to the dermis by thick bundles of Sharpey's fibers (e.g., Moss, 1969; Levrat-Calviac, 1986). It also fails to explain why ornamented bones in some taxa, such as most of the pseudosuchians (cf. Buffrénil et al., 2015), contain far less Sharpey's fibers than the bones of other taxa, like several turtles (this study), whereas they can display much sharper ornamental reliefs. At last, this interpretation does not address the question why ornamentation occurs in certain taxa and not in others, thus differing even between closely related taxa (e.g., among turtles, anurans, etc.), whereas there is no definite argument to settle that skin attachment on bone differs between them.

Beyond basal tetrapods, bone ornamentation has been shown in this study to be mainly caused by differential growth in a broad and diverse sample of gnathostome taxa, including actinopterygians (e.g., *Phractocephalus*), the finned sarcopterygian *Holoptychius*, the embolomere *Archeria,* and the Permian amniotes *Captorhinus* and *Lupeosaurus*. The involvement of this process was also reported

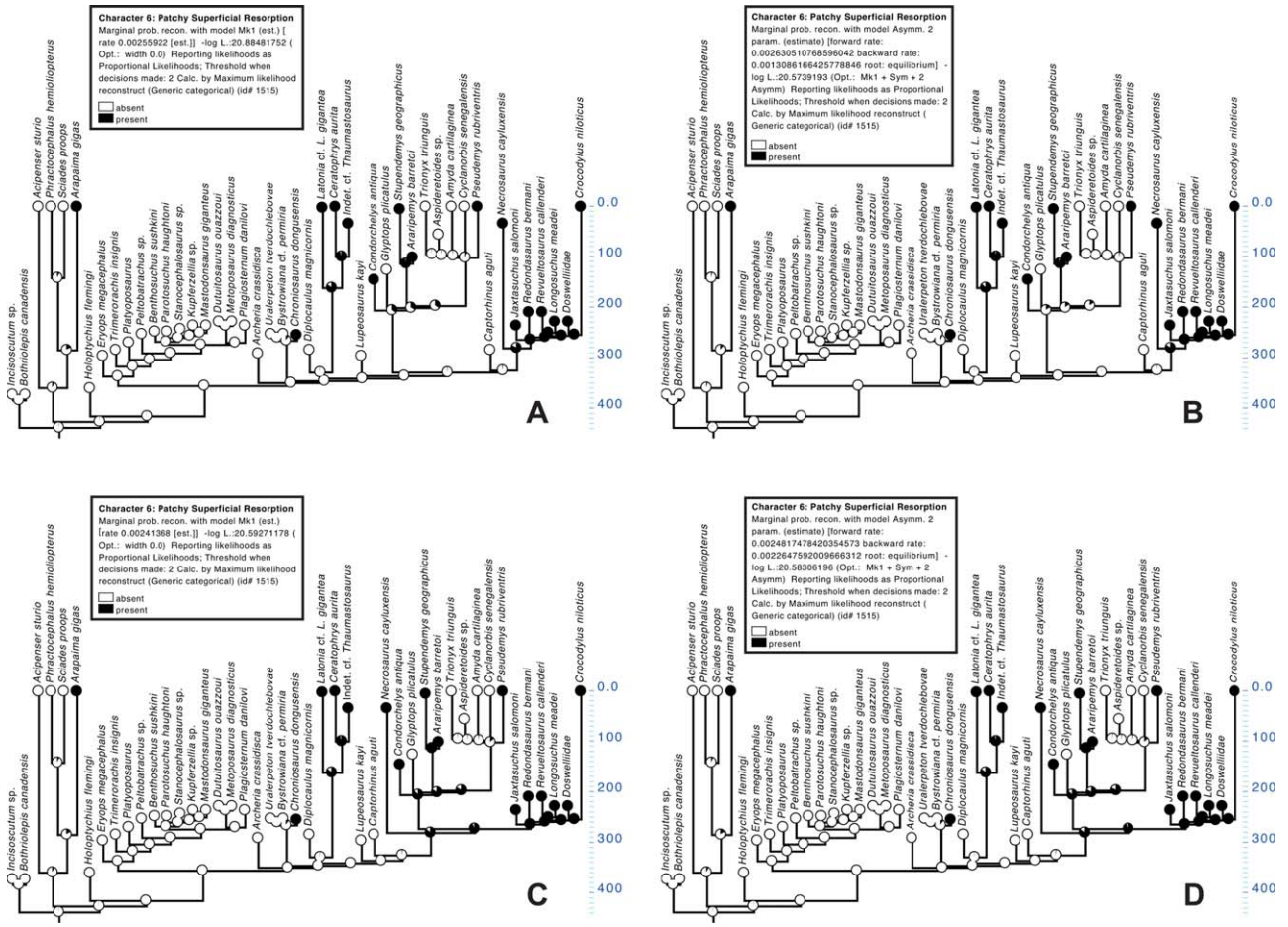

Fig. 17. Evolutionary pattern of the presence of patchy superficial resorption (character 6) in the developmental mechanism responsible for dermal ornamentation in gnathostomes. To make the tree more legible, the stratigraphic scale is omitted and is replaced by a simple absolute time scale. For more information, see legend of Figure 15. Optimization with turtles outside diapsids and a one-rate (**A**) and a two-rate (**B**) model, and with turtles in diapsids with a one-rate (**C**) and a two-rate (**D**) model.

in Devonian stem-gnathostomes, the placoderms, by Giles et al. (2013, see also Downs and Donoghue, 2009).

Turtle ornamentation involves local remodeling, whose interpretation has been problematic. Detailed histological studies of ornamented carapaces in various extant and extinct turtle taxa (e.g., stem-turtles, Trionychidae, Pelomedusidae, Podocnemidae, etc.) were recently conducted by Scheyer and Sánchez-Villagra (2007), Scheyer et al. (2007, 2012), and Cerda et al. (2015b). The occurrence of local remodeling, in the form of resorption and reconstruction topographically related to ornamentation, was mentioned and clearly illustrated in the trionychid *Aspideretoides* (Scheyer et al., 2012), the podocnemyd *Podocnemys erythrocephala*, the bothremydid (an extinct taxon) *Bothremys barbieri* (Scheyer et al., 2007), and the Jurassic stem turtle *Condorchelys antiqua* (Cerda et al., 2015b). However, an interpretation referring to pathological disorders was given to that observation: superficial carapace remodeling would reflect "a reaction to incipient osteomyelitis or *shell rot*" (Scheyer and Sanchez-Villagra, 2007). This interpretation, though in obvious contradiction with the highly organized geometrical pattern created by ornamentation, was later extended by Witzmann (2009) to the scarce phenomena of superficial resorption displayed by ornamented bones in basal tetrapods. This view explicitly refers (*op. cit*. p. 261) to the postulate that true (nonpathologic) bone ornamentation, whenever present, is mandatorily due to "preferential apposition" on ridges and, as such, represents a plesiomorphic character of tetrapods, deeply rooted within finned tetrapodomorphs. We concur that primitively in gnathostomes, resorption was apparently not involved in the development of dermal ornamentation, but not with the interpretation of a pathological nature of resorption (see below).

The process of preferential apposition on ridges is far from being the sole non-pathological mechanism susceptible to create ornamentation. The observations presented above reveal that superficial bone resorption, followed or not by secondary

reconstruction, is involved in 12 (including 6 turtles) of the 33 genera (one of which is not identified) sampled in this study. In addition, this process is a general feature of the pseudosuchians (Buffrénil et al., 2015), including the phytosaurs (Scheyer et al., 2014; Buffrénil et al., 2015), the aetosaurs (Cerda and Desojo, 2010), and the Dosweliidae (a taxon of Triassic archosauriformes: Cerda et al., 2015a). Moreover, the photographs of sections in the osteoderms of the chroniosuchians *Chroniosuchus dongusensis* and *Bystrowiella schumanni* published in Buchwitz et al. (2012) and Witzmann and Soler-Gijòn (2010) suggest that ornamentation in these taxa could also be due, at least partly, to superficial remodeling. It is noteworthy that the specimen of *Bystrowiana* used in the present study does not show evidence of a resorption process, as is also the case for the chroniosuchian *Uralerpeton tvedoschlebovae* described by Buchwitz et al. (2012). This question deserves further investigation. If the various contradictory observations relative to these taxa are confirmed by additional data, they would demonstrate that closely related forms can develop ornamentation through different mechanisms, a situation that precisely matches the observations presented above about the siluriforms *Phractocephalus* (in which only differential growth is involved) and *Sciades* (in which superficial bone remodeling occurs).

The discrepancies observed between various chroniosuchians could possibly reflect individual differences in calcium and phosphorus recycling (a process based on bone resorption), but this hypothesis is unlikely because the core of ornamented bones, which stocks much greater mineral reserves than their superficial layers for an obvious volumetric reason, is itself remodeled and already susceptible to contribute to calcium and phosphorus release. Thus, resorption involved in ornamentation development is unlikely to have appeared as a result of selective pressures to recycle mineral reserves. Finally, as properly pointed out by Cerda et al. (2015a), the formation of bone ornamentation "appears to be more complex than expected" and may respond to distinct immediate determinisms in the taxa that display it.

Our observations show a far more complex evolutionary pattern of the mechanisms responsible for the development of dermal sculpturing than we recently suggested (Buffrénil et al., 2015) based on a sample of Crurotarsi (Pseudosuchia). That study had suggested that the ornamentation found in Crurotarsi might not be homologous with that of most other gnathostomes because, contrary to the latter (represented only by a turtle and a temnospondyl, in our previous study), ornamentation of all sampled Crurotarsi (34 terminal taxa) involves resorption. However, we do confirm the primitive nature of the development of dermal sculpturing through differential apposition.

If the developmental mechanism is a guide to homology, our study identifies at least one other case in which ornamentation may not be homologous. Namely, the three sampled anurans have ornamentation associated with resorption. Given that most lissamphibian and many lepospondyl dermal bones lack ornamentation (Carroll and Gaskill, 1978; Laurin, 1998 [see character 3 in appendices 1 and 2 of that paper]), the occurrence of ornamentation in *Latonia*, *Ceratophrys*, and *Thaumastosaurus* may well result from one or several reappearances of ornamentation from ancestors with smooth dermal bones.

The other cases in which resorption appeared (Fig. 15) may not necessarily suggest that ornamentation in these taxa reappeared from unornamented ancestors because in teleosts and chroniosuchians dermal ornamentation is much more common. However, a comparative study with a much greater taxonomic sampling encompassing many unornamented taxa is needed to settle this question of historical (secondary) homology.

Functional Remarks

The role of bone ornamentation remains unclear. Since Bystrow's pioneer works (1935, 1947), at least five hypotheses have been proposed to explain the functional significance of this character. In brief, bone ornamentation could be involved in: a) reinforcement of skin anchorage onto bone (Witzmann, 2009; Witzmann et al., 2010), b) improvement of cutaneous respiration (Bystrow, 1947), c) prevention of blood acidosis (Janis et al., 2012), d)mechanical strengthening of the bones (Coldiron, 1974, Rinehart and Lucas, 2013) and, e) improvement of thermoregulation (Seidel, 1979; Clarac et al., 2015). Criticizing each of these hypotheses is beyond the scope of this article (see critical synthesis in Clarac et al. 2015). Recent studies by Rinehart and Lucas (2013) and Clarac et al. (2015) pointed out that most of these functional interpretations rely on the assumption that ornamentation was selected to increase the area of dermal bones; this increase can easily be quantified (Clarac et al., 2015). Therefore, the mechanisms controlling the size and geometric features of ornamental reliefs during growth, and thus the resulting gain in area of bone surface at every growth stage, represent key elements on which the results of the present study can yield some relevant information.

The two main processes creating bone ornamentation, i.e. differential growth (with or without absolute acceleration of bone apposition on ridges) and remodeling (resorption and re-deposition on the superficial cortex), have deep consequences on the general growth pattern of bone ornamentation, its consistency with the overall growth of the

bones, and the capacity of ornamental reliefs to be modified during ontogeny, at least regarding pit extension, shape and depth. A detailed study of crocodilian ornamentation (Buffrénil et al., 2015) shows that the initial creation of ornamental reliefs by local cortical resorption, and their subsequent growth by remodeling, are submitted to no geometric constraint since the global geometry of the ornamental pattern can be entirely modified through various processes. The ornamental pattern can indeed be altered by the excavation of new pits (resorption), rising or drifting of ridges (differential apposition) or entire filling of pits, independently of the anatomical limits of the bones, their shape, the level of their growth activity and, to some extent, the detailed characteristics of pre-existing reliefs. Conversely, ornamentation development resulting exclusively from differential growth is directly constrained by existing reliefs. Pits can then increase their individual dimensions (e.g., coping with growth of the entire body) only through the processes described above: divergent drift of ridges, or reduction of ridge width. An increase in pit size resulting from these processes is severely limited for two reasons: on the one hand, a divergent drift of the ridges framing an individual pit necessarily precludes the same phenomenon around the neighboring pits (competition for growth of neighboring pits); on the other hand, a pronounced reduction in ridge width should result, in a first time, in drastic thinning and, *in fine*, in stopping the increase in height of the ridges since width reduction cannot be indefinite.

Convergent models for explaining the geometric pattern of pit development on temnospondyl bones have been proposed by Witzmann et al. (2010) and Morkovin (2015). According to these models ornamentation initially consists of grooves delimited by long radial or sagittal ridges, depending on the shape of the bones. The grooves subsequently form pits by the development of short transverse ridges that transform a system of sub-parallel furrows into a honeycomb-like assemblage of roughly polygonal pits. The present study has shown that once the pits are set in place in temnospondyls, they can modify their size, shape or reciprocal position in limited proportions only with the sole mechanisms of ridge narrowing or drifting and, to a lesser extent, pit filling. In addition, this process is likely to be much slower than resorption-based mechanisms because, for a given volume of bone, the destructive action of osteoclasts is much faster than the constructive action of osteoblasts (e.g., Krstic, 1985). Both processes thus differ sharply in their capacities to control the morphological plasticity and the accommodation capabilities of bone ornamentation.

These considerations lead us to hypothesize that the mechanism that creates bone ornamentation through resorption and remodeling is more advantageous (if ornamentation must adjust through ontogeny to perform whatever its function may be) than the process that produces ornamentation solely by differential apposition. If this is correct, then the presence of the latter in some taxa must be a primitive character, whereas the former must be a more derived condition. We tested this hypothesis by verifying if the process based on resorption and remodeling appeared later than preferential apposition, and if there was a trend toward more resorption and remodeling over time.

Observation of the patterns on the timetrees (Figs. 15–17) is coherent with this hypothesis, with the absence of resorption and reconstruction being clearly the primitive condition, from the root of the tree (Gnathostomata) and well into Amniota, under both topologies and both evolutionary (one- and two rates) models used, for the nine variable characters analyzed here (Figs. 15–17). Furthermore, the ML models that presumably have the most reliable estimates further confirm this interpretation, with forward rates for these characters (numbers 2 and, to a lesser extent, 6) being greater than backward rates. However, our study cannot assess which selective advantages may be conferred by the presence of resorption in the development of dermal ornamentation. This topic would be best investigated using other approaches, such as experimentation.

ACKNOWLEDGMENTS

The authors are extremely grateful to all the colleagues who generously accepted to give or facilitate access to extant or fossil bone samples for this study: Salvador Bailon, Georges Bearez, Gaël Clément, France de Lapparent de Broin, François Meunier, Gabriella Prestes-Carneiro (all in the MNHN, Paris, France), Jean-Sébastien Steyer (CNRS/MNHN, Paris, France), Armand de Ricqlès (UPMC, Paris, France), Rainer Schoch (SMNS, Stuttgart, Germany), and Jean-Yves Sire (CNRS/UPMC, Paris, France). The authors also thank Vincent Rommevaux and Sophie Fernandez (MNHN, Paris, France) for their technical collaboration. The authors are grateful to two anonymous reviewers for their helpful comments and suggestions that improved this manuscript. The authors also thank the editor, Matthias Starck, for his efficient handling of the draft.

LITERATURE CITED

Amprino R. 1947. La structure du tissu osseux envisagée comme expression de différences dans la vitesse de l'accroissement. Arch Biol 58:315–330.

Amson E, Kolb C, Scheyer TM, Sánchez-Villagra MR. 2015. Growth and life history of middle Miocene deer (Mammalia, Cervidae) based on bone histology. C R Palevol 14:637–645.

Bollback JP. 2006. SIMMAP: Stochastic character mapping of discrete traits on phylogenies. BMC Bioinform 7:88.
Bolt JR. 1969. Lissamphibian origins: Possible protolissamphibian from the Lower Permian of Oklahoma. Science 166:888–891.
Buffrénil V de 1982. Morphogenesis of bone ornamentation in extant and extinct crocodilians. Zoomorphology 99:155–166.
Buffrénil V de, Rage J-C, Dauphin Y, Sire J-Y. 2011. An enamel-like tissue, osteodermine, on the osteoderms of a fossil anguid (Glyptosaurinae) lizard. C R Pale 10:427–438.
Buffrénil V de, Clarac F, Fau M, Martin S, Martin B, Pellé E, Laurin M. 2015. Differentiation and growth of bone ornamentation in vertebrates: A comparative histological study among the Crocodylomorpha. J Morphol 276:425–445.
Buchwitz M, Foth C, Kogan I, Voigt S. 2012. On the use of osteoderm features in a phylogenetic approach on the internal relationships of the Chroniosuchia (Tetrapoda: Reptiliomorpha). Palaeontology 55:623–640.
Bystrow AP. 1935. Morphologische Untersuchungen der Deckknochen des Schädels der Wirbeltiere. I. Mitteilung—Schädel der Stegocephalen. Acta Zool 16:65–141.
Bystrow AP. 1947. Hydrophilous and xerophilous labyrinthodonts. Acta Zool 28:137–164.
Carroll RL, Gaskill P. 1978. The Order Microsauria. Philadelphia: American Philosophical Society. 211 p.
Castanet J, Grandin A, Abourachid A, de Ricqlès A. 1996. Expression de la dynamique de croissance dans la structure de l'os périostique chez *Anas platyrhynchos*. C R Acad Sci III 319:301–308.
Castanet J, Rogers KC, Cubo J, Boisard J-J. 2000. Periosteal bone growth rates in extant ratites (ostriche and emu). Implications for assessing growth in dinosaurs. C R Acad Sci III 323:543–550.
Cerda IA, Desojo JB. 2010. Dermal armour histology of aerosaurs (Archosauria: Pseudosuchia), from the Upper Triassic of Argentina and Brazil. Lethaia 44:417–428.
Cerda IA, Desojo JB, Trotteyn MJ, Scheyer TM. 2015a. Osteoderm histology of *Proterochampsia* and Doswelliidae (Reptilia: Archosauriformes) and their evolutionary and paleobiological implications. J Morphol 276:385–402.
Cerda IA, Sterli J, Scheyer TM. 2015b. Bone shell microstructure of *Condorchelys antiqua* Sterli, 2008, a stem turtle from the Jurassic of Patagonia. C R Palevol 15:133–146.
Chiari Y, Cahais V, Galtier N, Delsuc F. 2012. Phylogenomic analyses support the position of turtles as the sister group of birds and crocodiles (Archosauria). BMC Biol 10:65.
Clack JA, Klembara J. 2009. An articulated specimen of *Chroniosaurus dongusensis* and the morphology and relationships of the chroniosuchids. Spec Pap Palaeontol 81:15–42.
Clarac F, Souter T, Cornette R, Cubo J, Buffrénil V de. 2015. A quantitative assessment of bone area increase due to ornamentation in the Crocodylia. J Morphol 276:1183–1192.
Coldiron RW. 1974. Possible function of ornament in the labyrinthodont amphibians. Occasional papers of the Museum of Natural History, the University of Kansas, Lawrence, Kansas, Vol. 33. pp. 1–19.
Cubo J, Le Roy N, Martinez-Maza C, Montes L. 2012. Paleohistological estimation of bone growth rate in extinct archosaurs. Paleobiology 38:335–349.
Currey JD. 2002. Bones, Structure and Mechanics. Princeton and Oxford: Princeton University Press.
Dacke CG. 1979. Calcium Regulation in Sub-Mammalian Vertebrates. London: Academic Press.
Danilov IG, Vitek NS. 2013. Soft-shelled turtles (Trionychidae) from the Bissekty Formation (Late Cretaceous: late Turonian) of Uzbekistan: Shell-based taxa. Cretac Res 41:55–64.
Downs JP, Donoghue PCJ. 2009. Skeletal histology of *Bothriolepis canadensis* (Placodermi, Antiarchi) and evolution of the skeleton at the origin of jawed vertebrates. J Morphol 270: 1364–1380.
Eltink E, Langer MC. 2014. A new specimen of the temnospondyl *Australerpeton cosgriffi* from the Late Permian of Brazil (Rio Do Rasto Formation, Paraná Basin): Comparative anatomy and phylogenetic relationships. J Vertebr Paleontol 34:524–538.
Francillon-Vieillot H, Buffrénil V de , Castanet J, Géraudie J, Meunier FJ, Sire J-Y, Zylberberg L, Ricqlès A de. 1990. Microstructure and mineralization of vertebrate skeletal tissues. In: Carter JG, editor. Skeletal Biomineralization: Patterns, Processes and Evolutionary Trends, Vol. 1. New York: Van Nostrand Reinhold. pp 471–530.
Germain D, Laurin M. 2009. Evolution of ossification sequences in salamanders and urodele origins assessed through event-pairing and new methods. Evol Dev 11:170–190.
Giles S, Rücklin M, Donoghue PCJ. 2013. Histology of the "placoderm" dermal skeletons: Implications for the nature of the ancestral gnathostome. J Morphol 274:627–644.
Gradstein FM, Ogg JG, Schmitz M, Ogg G, editors. 2012. The Geologic Time Scale 2012. Amsterdam: Elsevier. 1176 p.
Guillon J-M, Guéry L, Hulin V, Girondot M. 2012. A large phylogeny of turtles (Testudines) using molecular data. Contrib Zool 81:147–158.
Holmes R. 1989. The skull and axial skeleton of the Lower Permian anthracosauroid amphibian *Archeria crassidisca* Cope. Palaeontographica 207:161–206.
Hugall AF, Foster R, Lee MSY. 2007. Calibration choice, rate smoothing, and the pattern of tetrapod diversification according to the long nuclear gene RAG-1. Syst Biol 56:543–563.
Janis, CM, Devlin, K, Warren, DE, Witzmann, F. 2012. Dermal bone in early tetrapods: A palaeophysiological hypothesis of adaptation for terrestrial acidosis. Proc Biol Sci 279:3035–3040.
Josse S, Moreau T, Laurin M. 2006. Stratigraphic tools for Mesquite. Version 1.0. Available at http://mesquiteproject.org/packages/stratigraphicTools/
Karaplis AC. 2008. Embryonic development of bone and regulation of intramembranous and endochondral bone formation. In: Belezikian JP, Raisz G, Martin TJ, editors. Principles of Bone Biology, Vol. 1. Amsterdam: Academic Press. pp 53–84.
Kolb C, Scheyer TM, Lister AM, Azorit C, de Vos J, Schlingemann MAJ, Rössner GE, Monaghan NT, Sánchez-Villagra MR. 2015. Growth in fossil and extant deer and implications for body size and life history evolution. BMC Evol Biol 15:19–34.
Krstic RV. 1985. General Histology of the Mammal. Berlin: Springer Verlag.
Kumar S, Hedges SB. 2011. TimeTree2: Species divergence times on the iPhone. Bioinformatics 27:2023–2024.
Lamm E-T. 2013. Preparation and sectioning of specimens. In: Padian K, Lamm ET, editors. Bone Histology of Fossil Tetrapods. Berkeley: University of California Press. pp 55–160.
Landmann L. 1986. Epidermis and dermis. In: Bereiter-Hann J, Matoltsy AG, Richards KS, editors. Biology of the Integument, Vol. 2 Vertebrates. Berlin: Springer-Verlag. pp 150–187.
Laurin M. 1998. The importance of global parsimony and historical bias in understanding tetrapod evolution. Part I. Systematics, middle ear evolution, and jaw suspension. Annales Des Sciences Naturelles, Zoologie, Paris, 13e Série 19:1–42.
Laurin M. 2000. Seymouriamorphs. In: Heatwole H, Carroll RL, editors. Amphibian Biology. Chipping Norton: Surrey Beatty & Sons. pp 1064–1080.
Laurin M. 2008. The splendid isolation of biological nomenclature. Zool Scripta 37:223–233.
Laurin M, Reisz RR. 1995. A reevaluation of early amniote phylogeny. Zool J Linn Soc 113:165–223.
Lee MSY. 2001. Molecules, morphology, and the monophyly of diapsid reptiles. Contrib Zool 70:1–18.
Lee MSY. 2013. Turtle origins: Insights from phylogenetic retrofitting and molecular scaffolds. J Evol Biol 26:2729–2738.
Lehmann J-P. 1966. Actinoptérygiens, Dipneustes, Crossoptérygiens. In: Piveteau J, editor. Traité de Paléontologie, tome IV, Vol. 3. Paris: Masson. pp 1–412.
Levrat-Calviac V. 1986. Etude comparée des ostéodermes de *Tarentola mauritanica* et de *T. neglecta* (Gekkonidae, Squamata). Arch Anat Microsc Morphol Expérim 75:29–43.

Lyson TR, Bever GS, Bhullar B-AS, Joyce WG, Gauthier JA. 2010. Transitional fossils and the origin of turtles. Biol Lett 6:830–833.
Lyson TR, Sperling EA, Heimberg AM, Gauthier JA, King BL, Peterson KJ. 2012. MicroRNAs support a turtle + lizard clade. Biol Lett 8:104–107.
Maddison WP, Maddison DR. 2014. Mesquite: A modular system for evolutionary analysis. Version 3. Available at http://mesquiteproject.org
Margerie E de, Cubo J, Castanet J. 2002. Bone typology and growth rate: Testing and quantifying 'Amprino's rule' in the mallard (*Anas platyrhynchos*). C R Biol 325:221–230.
Margerie E de, Robin J-P, Verrier D, Cubo J, Groscolas R. 2004. Assessing the relationship between bone microstructure and growth rate: A fluorescent labeling study in the king penguin chick (*Aptenodytes patagonicus*). J Exp Biol 207:869–879.
Marjanović D, Laurin M. 2013. The origin(s) of extant amphibians: A review with emphasis on the "lepospondyl hypothesis". Geodiversitas 35:207–272.
Meunier FJ. 1984. Spatial organization and mineralization of the basal plate of elasmoid scales in osteichthyans. Amer Zool 24:953–964.
Meunier FJ, Castanet J. 1982. Organisation des fibres de collagène de la plaque basale des écailles des téléostéens. Zool Scripta 11:141–153.
Miles RS. 1967. Observations on the ptyctodont fish *Rhamphodopsis* Watson. J Linn Soc (Zool) 47:99–120.
Morkovin BI. 2015. On the development of surface ornamentation of skull bones in the ontogeny of Early Triassic Benthosuchids (Amphibia, Temnospondyli). Paleontol J 49:57–69.
Moss ML. 1969. Comparative histology of dermal sclerifications in reptiles. Acta Anat 73:510–533.
Oakley TH, Cunningham CW. 2000. Independent contrasts succeed where ancestor reconstruction fails in a known bacteriophage phylogeny. Evolution 54:397–405.
Padian K. 2013. Why study the bone microstructure of fossil tetrapods? In: Padian K, Lamm E-T, editors. Bone Histology of Fossil Tetrapods. Berkeley: University of California Press. pp 1–11.
Pagel M. 1999. The maximum likelihood approach to reconstructing ancestral character states of discrete characters on phylogenies. Syst Biol 48:612–622.
Pawley K. 2006. The Postcranial Skeleton of Temnospondyls (Tetrapoda: Temnospondyli) [PhD]. Melbourne, Australia: La Trobe University. 442 p.
Ricqlès A de, Meunier FJ, Castanet J, Francillon-Vieillot H. 1991. Comparative microstructure of bone. In: Hall BK, editor. Bone, 3: Bone Matrix and Bone Specific Products. Boca Raton: CRC Press. pp 1–78.
Rieppel O, Reisz RR. 1999. The origin and early evolution of turtles. Annu Rev Ecol Syst 30:1–22.
Rinehart LF, Lucas SG. 2013. The functional morphology of dermal bone ornamentation in temnospondyl amphibians. In: Tanner LH, Spielmann JA, Lucas SG, editors. The Triassic System. New Mexico Museum of Natural History and Science, Bull. 61. pp 524–532.
Ruta M, Coates MI. 2007. Dates, nodes and character conflict: Addressing the lissamphibian origin problem. J Syst Palaeontol 5:69–122.
Scheyer TM, Sánchez-Villagra MR. 2007. Carapace bone histology in the giant pleurodiran turtle *Stupendemys geographicus*: Phylogeny and function. Acta Palaeontol Pol 52:137–154.
Scheyer TM, Anquetin J. 2008. Bone histology of the Middle Jurassic turtle shell remains from Kirtlington, Oxfordshire, England. Lethaia 41:85–96.
Scheyer TM, Sander MP, Joyce WG, Böhme W, Witzel U. 2007. A plywood structure in the shell of fossil and living soft-shelled turtles (Trionychidae) and its evolutionary implications. Org Divers E 7:136–144.
Scheyer TM, Mörs T, Einarsson E. 2012. First record of soft-shelled turtles (Cryptodira, Tryonychidae) from the Late Cretaceous of Europe. J Vert Paleontol 32:1027–1032.
Scheyer TM, Desojo JB, Cerda IA. 2014. Bone histology of phytosaur, aetosaur, and other archosauriform osteoderms (Eureptilia, Archosauromorpha). Anat Rec 297:240–260.
Schluter D, Price T, Mooers AØ, Ludwig D. 1997. Likelihood of ancestor states in adaptive radiation. Evolution 51:1699–1711.
Schoch RR. 2008. The Capitosauria (Amphibia): Characters, phylogeny, and stratigraphy. Palaeodiversity 1:189–226.
Schoch RR. 2013. The evolution of major temnospondyl clades: An inclusive phylogenetic analysis. J Syst Palaeontol 11:673–705.
Schoch RR, Milner AR. 2000. Stereospondyli. Handbuch der Paläoherpetologie, Teil 3B. München: Verlag Dr. Friedrich Pfeil. 203 p.
Schoch RR, Milner AR. 2014. Temnospondyli. In: Sues HD, editor. Handbook of Paleoherpetology, Part 3A2. München: Verlag Dr. Friedrich Pfeil.
Schoch RR, Sues H-D. 2015. A Middle Triassic stem-turtle and the evolution of the turtle body plan. Nature 523:584–587.
Schoch RR, Voigt S, Buchwitz M. 2010. A chroniosuchid from the Triassic of Kyrgyzstan and analysis of chroniosuchian relationships. Zool J Linn Soc 160:515–530.
Seidel, MR. 1979. The osteoderms of the American alligator and their functional significance. Herpetologica 35:375–380.
Sigurdsen T, Green DM. 2011. The origin of modern amphibians: A re-evaluation. Zool J Linn Soc 162:457–469.
Smith HF, Parker WH, Kotzé SH, Laurin M. 2013. Multiple independent appearances of the cecal appendix in mammalian evolution and an investigation of related ecological and anatomical factors. C R Palevol 12:339–354.
Sterli J, Pol D, Laurin M. 2013. Incorporating phylogenetic uncertainty on phylogeny-based paleontological dating and the timing of turtle diversification. Cladistics 29:233–246.
Swofford DL, Maddison WP. 1987. Reconstructing Ancestral character states under Wagner Parsimony. Math Biosci 87: 199–229.
Vallin G, Laurin M. 2004. Cranial morphology and affinities of *Microbrachis*, and a reappraisal of the phylogeny and lifestyle of the first amphibians. J Vert Paleontol 24:56–72.
Vickaryous MK, Hall BK. 2008. Development of the dermal skeleton in *Alligator mississippiensis* (Archosauria, Crocodylia) with comments on the homology of osteoderms. J Morph 269:398–422.
Vickaryous MK, Sire J-Y. 2009. The integumentary skeleton of tetrapods: Origin, evolution and development. J Anat 214: 441–464.
Wagenmakers E-J, Farrell S. 2004. AIC model selection using Akaike weights. Psychon Bull Rev 11:192–196.
Webster AJ, Purvis A. 2002. Testing the accuracy of methods for reconstructing ancestral states of continuous characters. Proc R Soc Lond B 269:143–149.
Witzmann F. 2009. Comparative histology of sculptured dermal bones in basal tetrapods, and the implications for the soft tissue dermis. Paleobiodiversity 2:233–270.
Witzmann F, Soler-Gijón R. 2010. The bone histology of osteoderms in temnospondyl amphibians and in the chroniosuchian *Bystrowiella*. Acta Zool 91:96–114.
Witzmann F, Scholz H, Müller J, Kardjilov N. 2010. Sculpture and vascularization of dermal bones, and the implications for the physiology of basal tetrapods. Zool J Linn Soc 160:302–340.